Detection and tracking of mesoscale eddies in the Mediterranean Sea: A comparison between the Sea Level Anomaly and the Absolute Dynamic Topography fields

Cori Pegliasco, Alexis Chaigneau, Rosemary Morrow, Franck Dumas

Version of Record: https://www.sciencedirect.com/science/article/pii/S027311772030212X
Manuscript_8d877a600ac37e38b036906c2bdbd1b9

Detection and tracking of mesoscale eddies in the Mediterranean Sea : A comparison between the Sea Level Anomaly and the Absolute Dynamic Topography fields

Cori Pegliasco [1]*, Alexis Chaigneau [1], Rosemary Morrow [1], Franck Dumas [2]

[1] Laboratoire d'Etudes en Géophysique et Océanographie Spatiales (LEGOS) / UMR CNRS / Université Paul Sabatier / CNES / IRD, Toulouse, France

[2] Service Hydrographique et Océanographique de la Marine (SHOM), Brest, France

* Corresponding author:

LEGOS, 14. Av. Edouard Belin, 31400 Toulouse, France

SHOM, 13 rue du Chatellier, 29200 Brest

Telephone: (+33) 5 61 33 30 03

cori.pegliasco@legos.obs-mip.fr

Co-authors:

Alexis Chaigneau: alexis.chaigneau@legos.obs-mip.fr

Rosemary Morrow: rosemary.morrow@legos.obs-mip.fr

Franck Dumas: franck.dumas@shom.fr

Service Hydrographique et Océanographique de la Marine

13 rue du Châtellier, 29200 Brest, France

Abstract:

Mediterranean Sea eddies are often generated in fixed geographical locations linked to bathymetric or coastline changes, instabilities around islands or from orographic wind forcing. Because of that, the mean circulation exhibits features with the same special scales as the mesoscale field. We provide here a first comparison of eddies detected and tracked using two altimetry products, the Sea Level Anomaly (SLA) and the Absolute Dynamic Topography (ADT), from 2000 to 2015. We showed that more individual eddies and trajectories are detected in the SLA data than in the ADT, having larger radius but lower Eddy Kinetic Energy. The spatial distribution of the mesoscale activity is different between the two data sets: the ADT-detected eddies closely follow the Mean Dynamic Topography (MDT) patterns which include the mean eddy generation sites whereas the SLA-detected eddies show more spatial homogeneity. The larger eddies are generally well detected in both the ADT or the SLA fields, but the numerous smaller and coastal eddies detected in the SLA fields have a tendency to mismatch the ADT detected eddies. Only 20 – 30 % of eddies are detected exclusively in the SLA or the ADT product (i.e. have no collocation in the other field), whereas to 65 – 80 % of the eddies are detected both in the SLA and the ADT fields. The Ierapetra Eddy is a typical example of the limitation of the SLA-detected eddies, as this orographically controlled feature is present in the MDT and thus leads to an artificial cyclonic eddy in the SLA field that shifts around its most frequent position.

This study recommends the use of ADT fields for the detection of mesoscale structures in the Mediterranean Sea where the mean circulation and these mesoscale features have the same spatial scale and intensity, and similarly for any other ocean regions where the MDT contains mesoscale patterns. Yet the ADT fields depend on the accuracy of the MDT, and the altimeter-based SLA fields may be preferable in specific locations where the MDT is not reliable.

Keywords: altimetry; mesoscale eddies; Mediterranean Sea; sea level

1. Introduction

Altimetric fields of Sea Surface Height (SSH) are widely used to study mesoscale eddies during their lifetime in the open ocean (Chaigneau et al., 2008; Chelton et al., 2011, 2007; Dong et al., 2014, 2012; Halo et al., 2014; Kurian et al., 2011; Le Vu et al., 2018; Mason et al., 2014; Yi et al., 2014). The detection and tracking methods can be based on different techniques: geometrical (Dong et al., 2012; Mkhinini et al., 2014; Nencioli et al., 2010; Sadarjoen and Post, 2000) or physical (Chelton et al., 2007; d'Ovidio et al., 2009; Doglioli et al., 2007; Isern-Fontanet et al., 2003; Morrow et al., 2004), or both (Chaigneau et al., 2008; Chelton et al., 2011; Dong et al., 2014; Halo et al., 2014; Kurian et al., 2011; Le Vu et al., 2018; Mason et al., 2014; Yi et al., 2014). The ability to track the pathways of these open ocean mesoscale eddies is important in order to quantify how the coherent vortices transport physical and bio-geochemical tracers trapped in their cores across oceans, between their generation regions and their dissipation areas.

In the open ocean, Sea Level Anomaly (SLA) fields are widely used to detect and track these mesoscale eddies (Chaigneau et al., 2008, 2009; Chelton et al., 2011, 2007; Dong et al., 2014; Mason et al., 2014; Morrow et al., 2004; Pegliasco et al., 2015; Yi et al., 2014). By construction of the SLA field, mesoscale eddies detected in it are anomalies from the mean circulation. In certain open ocean regions, features in the large-scale mean circulation have similar spatial scales to the mesoscale eddies. In these regions, other authors have applied eddy detection algorithms to the Absolute Dynamic Topography field (ADT) containing the Mean Dynamic Topography (MDT) and its variability (i.e. the SLA). For example in the South East Atlantic, the Agulhas Retroflection exhibits a strong geographical pattern in the mean circulation and its variability, leading to the formation of large

anticyclonic eddies, which have been studied via the ADT field (Doglioli et al., 2007; Laxenaire et al., 2018; Rubio et al., 2009). In the Mozambique Channel, a narrow passage where eddies can develop, de Ruijter et al. (2002) found that the movement of cyclonic eddies detected in SLA maps did not match with *in situ* measurements, in contrast to the anticyclonic eddies. Schouten et al. (2003) stated that "the frequent passage of positive anomalies through the Mozambique Channel leaves a signal in the mean SSH field, leading to negative SLAs when no anticyclone is present". In the same region, Halo et al. (2014) also stated that the eddy's detection with ADT fields "prevents the spurious detection of current meanders, which are often associated with closed sea level anomaly loops".

Semi-enclosed seas, such as the Mediterranean Sea, also exhibit mesoscale activity and a mean circulation with similar spatial scales, but in contrast to the open ocean, both dynamical components are highly constrained by the basin morphology (coasts, islands, shelf breaks) and the meterological forcing over the mountainous orography. In the Mediterranean Sea, the kinetic energy is slightly higher for the mesoscale anomalies (EKE for Eddy Kinetic Energy, Figure 1a) than for the mean circulation (MKE for Mean Kinetic Energy, Figure 1b), derived here from the Mean Dynamic Topography (MDT) produced by Rio et al. (2014) and reproduced in Figure 2.

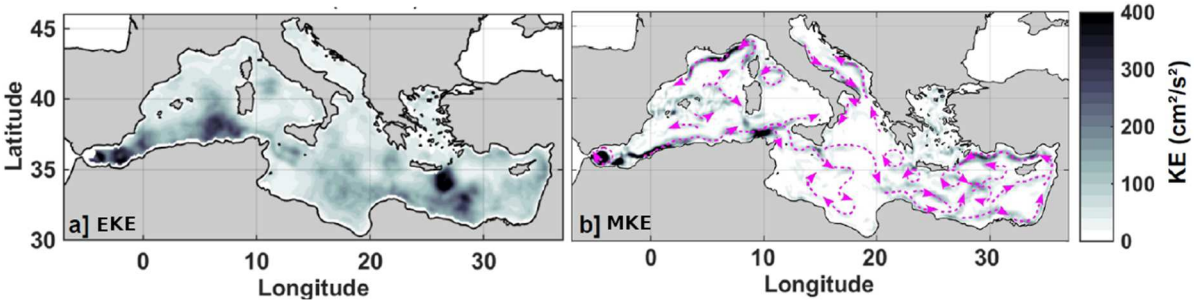

Figure 1 : Averaged Kinetic Energy (KE) associated with **a]** *the mesoscale activity (2000 – 2015) and* **b]** *the mean circulation derived from the MDT. The pink arrows highlight the more energetic pathways of the mean circulation.*

In contrast to the open ocean, the mean circulation of the Mediterranean Sea (Figure 2) is composed of features having the same spatial scale as the instantaneous mesoscale field. Thus, separating the transient mesoscale field from the more recurrent features is not trivial. Even the terms "eddies" and "gyres" can cover similar scales in Mediterranean Sea. Mesoscale eddies are coherent rotating structures, that can propagate, guided or not by the topography, and transport water away from their generating area to their dissipating zone. In contrast, gyres can be associated with wind- or topographic-driven closed circulations (Hamad et al., 2006). As several recurrent or permanent eddies and gyres imprint their signature within the MDT (Figure 2, Amitai et al., 2010), the Sea Surface Height (SSH) field used for the eddy detection will include transient or more recurrent features.

The question of the aptitude of SLA to describe the mesoscale eddies in the Mediterranean Sea arose with Isern-Fontanet et al. (2006), when they highlighted the presence of intense cyclonic vortices in the SLA fields at the position of quasi-permanent anticyclones (e.g. the Ierapetra Eddy location and the Eastern Alboran Gyre). The difficulty to interpret SLA is clearly stated by Rio et al. (2007) : positive anomalies can either be associated with an anticyclonic eddy, the strengthening of a quasi-permanent anticyclonic eddy or meander, the decay of a cyclonic eddy or meander, the meandering or the spatial shift of a current. The opposite applies for negative sea level anomalies.

In addition to the choice of using SLA or ADT altimetric fields for these eddy studies, numerous detection and tracking methods can be applied. Intercomparisons between some of these different eddy detection and tracking techniques have been previously made in different regions (e.g. Escudier et al., 2016; Souza et al., 2011). In general, although the large open-ocean eddies are well tracked by most methods, there are differences in the detection and tracking capabilities of smaller from one method to another.

As the Mediterranean Sea contains both quasi-permanent mesoscale features and strong alongshore currents, this paper will concentrate on providing a first description of the eddy detection and tracking capabilities when starting from SLA or ADT fields, with a particular consideration for the Ierapetra Eddy. We will use one eddy-detection and tracking scheme based on local SSH extrema, following Chaigneau et al. (2008, 2009), and Pegliasco et al. (2015) which has been tested an analysed in many diverse regions (described in Pegliasco et al., 2015).

This paper is organized as follows. In section 2, we present the major Mediterranean mesoscale features. In section 3, the data and methods are described. In section 4, we first investigate how the the eddies' surface characteristics are detected in the SLA and the ADT fields; then we provide a direct comparison of the eddies detected in the mapped SLA and ADT fields, with a focus on the Ierapetra Eddy. In section 5, we discuss the reliability of the representation of the smallest structures and the capacity of the two fields to observe the recurrent and transient mesoscale features in different regions. We provide a summary of our work in section 6.

2. Background details of major Mediterranean Eddies

Over its whole domain, the Mediterranean Sea exhibits a large-scale cyclonic circulation that is also present in each of its sub-basins, as described by Poulain et al. (2012). We review here the main features of the Mediterranean sub-basins, from West to East. The positions of the main eddies are marked in Figure 2.

The most energetic peak of the basin-scale mean circulation highlights the presence of the **Western Alboran Gyre**, in the Alboran Sea, located just East of the Gibraltar Strait (Figure 1b). This anticyclonic feature is strongly constrained by the coastline, the bathymetry of the Alboran Sea and the density difference between the light Atlantic Water and the denser Mediterranean Water (Wang, 1987), and it appears clearly in the MDT (Figure 2). The EKE,

derived from the Sea level Anomaly (SLA) maps from 2000 – 2015 (Figure 1a), also exhibits a large amount of variable energy in the Western Alboran Gyre and from its neighbor the Eastern Alboran Gyre (Heburn and La Violette, 1990; Poulain et al., 2012; Vargas-Yáñez et al., 2002; Viúdez et al., 1996). In the Algerian Basin, the eastward current flowing along the African coast is responsible for a strong gradient in the MDT between the shoreline and the open waters. This Algerian Current is unstable and develops large anticyclonic meanders that eventually separate from the coast and become open ocean large eddies (Millot, 1985; Obaton et al., 2000; Pessini et al., 2018; Puillat et al., 2002; Salas et al., 2002, 2003; Taupier-Letage, 2003).

In the Tyrrhenian Sea west of Italy, the position of the cyclonic part of the Bonifacio dipole (BE, **Bonifacio Eddy**, 10°E, 41.5°N), mainly due to the wind stress curl (Millot and Taupier-Letage, 2005), is visible both in the mean and the eddy kinetic energy (Figure 1). The anticyclonic part of this dipole located South of the BE is visible in both the MKE and MDT. Between the Capraia and Elba islands (~10°E, 43°N, off the north-western coast of Italy), an anticyclonic circulation of about 40 km in diameter, named the **Capraia Eddy**, is fairly stable, with a weak imprint in the MDT, but not in the KE (Onken et al., 2005; Robinson et al., 2002).

In the Liguro-Provençal Basin south of France, the Northern Current has a strong signature in the MKE, whereas the southern branch of the basin-wide cyclonic circulation is weaker. The Northern Current, flowing alongshore from France to Spain, exhibits a strong mesoscale variability, in particular in winter, when large meanders develop (Echevin et al., 2003; Millot, 1999), but has only low levels of EKE (Figure 1). The dense waters of the Liguro-Provençal Basin have a low MDT level, and drifters circulate around but do not penetrate in the lowest part (Poulain et al., 2012), whereas in the SLA, many anticyclonic eddies (AEs) and cyclonic eddies (CEs) are detected at the same place (Escudier et al., 2016;

Isern-Fontanet et al., 2006). The North Balearic Front (NBF), flowing eastward from the Balearic Islands towards Corsica, behaves as a barrier for the eddies coming from the Algerian Basin or the Catalan Sea (Echevin et al., 2003). It also generates eddies locally (Pessini et al., 2018). The NBF is visible as a blurred pattern in KE.

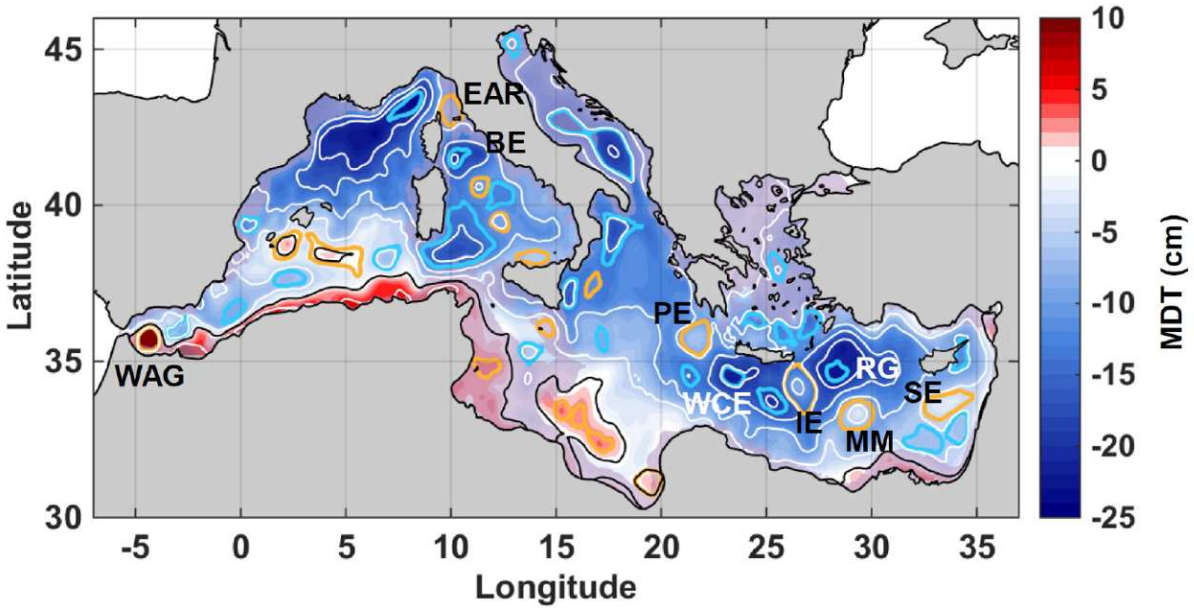

Figure 2 : *Mean Dynamic Topography (cm) over the Mediterranean Sea and associated closed contours for the mean anticyclonic (orange) and cyclonic (cyan) circulations. The white contours are every 5 cm and the black contour is for 0 cm. The light purple shading represents the bathymetry between the surface and 500 m depth. The main known features are designated as WAG: Western Alboran Gyre; CE: Capraia Eddy; BE: Bonifacio Eddy; PE: Pelops Eddy; WCE: Western Cretan Eddy; IE: Ierapetra Eddy; MM: Mersa-Matruh; RG: Rhodes Gyre; SE: Shikmona Eddy.*

In the Ionian Basin, a mesoscale anticyclonic circulation located South of the Peloponnese corresponds to the presence of the regularly observed **Pelops Eddy** (Malanotte-Rizzoli and Bergamasco, 1989; Matteoda and Glenn, 1996; Mkhinini et al., 2014; Poulain et al., 2012; Robinson et al., 1991; Theocharis et al., 1993), with a signature in the mean and the eddy kinetic energy (Figure 1), and the MDT. This structure seems to be generated in summer

due to wind stress curl produced by the Etesian winds over the Peloponnese orography (Ayoub et al., 1998; Horton et al., 1994; Mkhinini et al., 2014). In the MKE, the current entering the Ionian basin has a southern branch exhibiting meanders before completing an anticyclonic circulation corresponding to high values in the MDT. The northern branch crosses the basin to feed the Lybio-Egyptian Current, flowing eastward in the Levantine Basin. Part of this current detaches from the coast and crosses the basin via complex paths still under debate in the literature; another part flows alongshore, to finally form a Northern Current along the Turkish coast, named the Asia Minor Current. South of the island of Crete, the signatures of the **Western Cretan Eddy**, a cyclonic mesoscale structure present at its southwestern corner, and of the **Ierapetra Eddy**, an anticyclonic feature located at its southeastern corner, are visible in the MKE and the MDT, but only the Ierapetra Eddy exhibits a strong imprint in the EKE (Figure 1). The Western Cretan Eddy is likely due to the Etesian winds (Matteoda and Glenn, 1996; Mkhinini et al., 2014; Theocharis et al., 1993), and could form a dipole with the Pelops Eddy (Hamad et al., 2006). It is depicted as a permanent gyre by some authors (Robinson et al., 1991; Theocharis et al., 1993) consistent with the low EKE. The Ierapetra Eddy is the most permanent feature in the Levantine basin. It is generated and energised by the wind stress curl associated with the Etesian winds over the Cretan orography almost every year in summer or fall (Amitai et al., 2010; Hamad et al., 2006; Horton et al., 1994; Ioannou et al., 2017; Mkhinini et al., 2014).

Another anticyclonic mesoscale feature, located off Mersa-Matruh and centered at 29°E, 33-34°N, is visible in the two kinetic energy fields and identified in the MDT. This feature is sometimes called the Mersa-Matruh gyre (Malanotte-Rizzoli and Bergamasco, 1989; Robinson et al., 1991), or is depicted as a complex system of several anticyclonic eddies (Amitai et al., 2010; Ayoub et al., 1998; Hamad et al., 2006; Horton et al., 1994; Ioannou et al., 2017; Millot and Taupier-Letage, 2005; Özsoy et al., 1989; Poulain et al.,

2012), or as a permanent eddy (Menna et al., 2012; Zervakis et al., 2003). In a similar way, the anticyclonic feature located South of Cyprus and centered at 33°E, 34°N is a place where several anticyclonic eddies have been found and can interact (Hamad et al., 2006; Menna et al., 2012; Millot and Taupier-Letage, 2005; Mkhinini et al., 2014) rather than a gyre. It contains the Cyprus Eddy, a recurrent anticyclone (Hamad et al., 2006; Menna et al., 2012; Zodiatis et al., 2005). Despite a closed anticyclonic circulation identified in the MDT, the MKE does not highlight it (Figure 2). Hecht et al. (1988) provided a detailed description of isolated and persistent vortices in this region, from a dataset of CTD casts launched from the *R/V Shikmona*, and the eddies generated in this area are often named Shikmona Eddies.

The **Rhodes Gyre**, located between Cyprus and Rhodes islands, is a large (~300 km diameter), persistent and multi-centered cyclonic circulation (Malanotte-Rizzoli and Bergamasco, 1989; Özsoy et al., 1989; Theocharis et al., 1993), clearly visible in the MDT and in the MKE but absent in the EKE. There is still a debate on this feature : Hamad et al. (2006) do not consider it as a gyre *stricto sensu* but rather as an association of the edges of different neighboring anticyclonic eddies in its southern part and of the westward alongshore current off Turkey in its northern part, whereas Menna et al. (2012) and Poulain et al. (2012) depict it as a gyre.

Despite its shallow depth, the cyclonic circulation in the Adriatic Sea is present in the MKE. Finally, the topography and the islands of the Aegean Sea are too complex to be represented with accuracy in the altimetric gridded products used in this paper and will not be investigated here.

This description shows that the Mediterranean Sea has a complex series of transient and recurrent features in each of the different basins. It is difficult to distinguish them using the assumption that recurrent features will be mostly present in the MDT and the MKE, and the transient eddies will appear mostly in the EKE. In our analysis, we will see how the two

altimetric products, with or without the mean circulation, represent this rather complex circulation variability.

3. Data and methods

3.1. Altimetry products

The mesoscale eddies are detected on two different datasets, the SLA and the ADT. These fields are made available by the European Copernicus Marine Service (marine.copernicus.eu) for the Mediterranean Sea as a regional gridded multi-missions altimeter product with a 1/8° spatial resolution and daily fields (Pujol and Larnicol, 2005). We have extracted a 15.5 year time series for our analysis from the 1st of January of 2000 to the 11th of September of 2015 of the DT2014 version (Pujol et al., 2016); this long series provides statistical robustness and covers a large range of interannual conditions. The construction of the SLA is described precisely in Pujol et al. (2016). The along-track SLA is the instantaneous Sea Surface Height (SSH) minus a temporal mean reference. This reference can either be a Mean Profile, the temporal averaged profile built for each mission on each repeated track, or the gridded Mean Sea Surface (MSS) when mean repeated profiles are not available, derived from other mean profiles and data from the geodetic phase of different altimetric missions. The along-track data are filtered with a Lanczos filter of 40 km and subsampled at 14 km in the Mediterranean Sea to reduce the residual noise; this process also filters out the small-scale signals. The gridded maps of SLA are produced for each date using an optimal interpolation with the best decorrelation scales for the Mediterranean Sea (100 km and 10 days, smaller than those used for the global map, Pujol and Larnicol, 2005).

The ADT is the sum of the gridded SLA and the Mean Dynamic Topography (MDT). The MDT represents the 20-year permanent ocean circulation, corresponding theoretically to the difference between the Mean Sea Surface Height and the marine geoid. Unfortunately, the

geoid cannot be measured with enough spatial accuracy to use it directly in the MDT calculation. Instead, the MDT is estimated from numerical simulations and *in situ* datasets: a first guess is obtained using an ocean circulation model, and then improved by *in situ* observations to obtain the best estimate possible (Rio et al., 2014). Hereafter, when we refer to both the ADT and the SLA fields, we will call them SSH.

These products mainly resolve the larger Mediterranean eddies. Even for along-track satellite data, altimetry can only resolve structures of 20 – 25 km in diameter in winter, and more than 25 km in diameter in summer (Morrow et al., 2017). Despite the finer resolution of the Mediterranean gridded regional product compared with the ¼° resolution in the open ocean, its wavelength effective resolution is still only ~100 km (i.e., 50 km diameter eddies) (Ballarotta et al., 2019; Pascual et al., 2015) whereas the typical internal Rossby radius in the Mediterranean sea ranges between 5 – 18 km (Damien, 2015; Escudier et al., 2016; Robinson et al., 2001; Rogé et al., 2017). Thus, the regional SSH products cannot represent the smaller mesoscale activity over the Mediterranean Sea; comparisons with *in situ* data highlight the lack of accuracy of the altimetry field, in particular in coastal regions (Escudier et al., 2013; Nencioli et al., 2011; Pascual et al., 2013). The smallest features detected in these SSH maps (radius ~ 10 km) could be realistic, more or less smoothed by the optimal interpolation, or artifacts created during the mapping within the gaps.

3.2. Eddy detection and tracking

In this study, we use a detection and tracking algorithm, based on the detection of a local extrema in the SSH field (minima for cyclonic eddies, maxima for anticyclonic eddies, see Chaigneau et al. 2008, 2009) and tracking following Pegliasco et al. (2015). Escudier et al (2015, 2016) showed that three different methods applied on the SLA fields (Chelton et al.,

2011; Halo et al., 2014; Nencioli et al., 2011) have consistent results in the Western Mediterranean Sea in terms of eddy's detection and physical characteristics. Moreover, we obtain similar detection and tracking of eddies when comparing our method with the recent AMEDA dataset based on closed velocity contours (Le Vu et al., 2018; Stegner and Le Vu, 2019: **https://doi.org/10.14768/2019130201.2**) for the same period, both based on the ADT fields (not shown).

Our detection algorithm (Chaigneau et al., 2008, 2009) looks for the outermost closed contour of SSH encircling only one local extrema. The local extrema are the centers of the detected eddies, and the last closed contour of SSH is their edge. The amplitude of an eddy is defined by the difference of SSH between its edge and its center, in absolute value. The radius associated with a circle of the same area as the considered eddy is its axisymmetric equivalent radius. The EKE of the eddy is the averaged value within the eddy's contour. No thresholds are applied on the radius nor the amplitude during the eddy detection stage.

The tracking algorithm (Pegliasco et al., 2015) looks for the possible overlapping contours of eddies on two different consecutive maps (see Figure 1 of Pegliasco et al. (2015). While a contour in a new map overlaps the previous one, the corresponding eddy is added to the trajectory. We allow the algorithm to search for an intersection over 10 days t+Ndt, with N = 1:10 and dt = 1day. This avoids the "missing eddy" problem, due to the possibility that an eddy passes between grounded tracks for a few days (Le Vu et al., 2018). If at t+10dt no contour is found, the trajectory is stopped. In the case of two or more overlapping contours, an improved cost function (CF) is applied, including the distance between the eddy centers. The most likely eddy to follow is when this CF is minimum :

$$\sqrt{\left(\frac{\Delta R-\overline{\Delta R}}{\sigma_{\Delta R}}\right)^2+\left(\frac{\Delta A-\overline{\Delta A}}{\sigma_{\Delta A}}\right)^2+\left(\frac{\Delta EKE-\overline{\Delta EKE}}{\sigma_{\Delta EKE}}\right)^2+\left(\frac{\Delta dist-\overline{\Delta dist}}{\sigma_{\Delta dist}}\right)^2} \qquad (1)$$

where ΔR, ΔA, and ΔEKE are the differences between the vortex delimited by C_t and those intersecting C_t at time $t+dt$ for, respectively, the radius, the amplitude, and the eddy kinetic energy, *dist* is the distance between the centers differences. Their averaged values are calculated for a set of ~1000 trajectories obtained with the single contour intersections; and σ corresponds to the standard deviation of the variations of the same set of trajectories.

3.3. Merging and splitting events

One challenge is to take into account the eddies' interactions: merging events occur when two or more eddies aggregate to form a larger eddy (Mkhinini et al., 2014; Taupier-Letage, 2008) and splitting events occur when a large eddy separates in two or more eddies (Ikeda, 1981). Recently, the characterization of merging and splitting events in a tracking algorithm was described (Le Vu et al., 2018; Li et al., 2016). Within our tracking algorithm, we record the merging and splitting events in a similar way to Li et al. (2016). When the overlapping contour at $t+N.dt$ is already associated with a trajectory, we identify this as a merging. We store the identities of the two trajectories, the main one and the merged one, and the time of the merging event. When two or more overlapping contours are found at $t+N.dt$, the cost function adds the more similar eddy to the trajectory, but we consider that the other eddies are split from the main trajectory. We record the identities of the main trajectory and the trajectories split from it as a splitting event. Due to the high number of interactions, a trajectory split from a main trajectory can merge with the same or another trajectory. Both events are then recorded as well.

We consider that a main trajectory has a generation and a dissipation position, whereas a merged trajectory has a generation and a merging position, a split trajectory has a split position and a dissipation position, and a split and merged trajectory has both a splitting and merging position. We note that the main trajectories represent ~70 % of the total trajectories, and up to 80 % of the total AEs trajectories in the ADT field.

3.4. Selection of the trajectories

		SLA		ADT	
	Trajectories Lifetimes	AEs	CEs	AEs	CEs
Individual eddies (snapshots)	**< 15 days (~20 %)**	111268	121797	85488	104654
	≥ 15 days (~80 %)	440751	464578	364735	462193
Trajectories (dynamic view)	**< 15 days (~75 %)**	30964	33613	22589	28368
	≥ 15 days (~25 %)	9252	10271	7411	9940

Table 1: Contribution of the number of individual eddies to trajectories lasting less or at least 15 days and the associated number of trajectories in the SLA and the ADT dataset.

Several eddy-detection algorithms include thresholds on different parameters in order to keep only eddies with a certain intensity, resulting in a large range of parameters that can be used, such as amplitude (Chaigneau et al., 2011), radius of maximum velocity (Mkhinini et al., 2014) or the Okubo-Weiss parameter (Chaigneau et al., 2008; Chelton et al., 2007; Isern-Fontanet et al., 2006). Such thresholds tend to discard the smaller and less intense eddies in each map. However, since the eddy amplitude is also smaller during the important growing and decay phases (see Figure 3) (Isern-Fontanet et al., 2006; Pegliasco et al., 2015; Samelson et al., 2014), we have chosen to use all amplitudes but select instead the trajectories that last at least 15 days. This value is of the same order of magnitude as the median lifetime of the altimetry-detected eddies in the Mediterranean Sea which is 13 days (Escudier et al., 2016), and is slightly longer than the altimetry mapping decorrelation time of 10 days used for the Mediterranean product (Dibarboure et al., 2011; Pujol and Larnicol, 2005).To be more specific, a main trajectory lasting less than 15 days or a merged/split trajectory shorter than 15 days are discarded from the dataset.

Following these restrictions, the algorithm detects more individual eddies from the SLA fields than from the ADT ones (Table Table 1). More trajectories are detected as well within the SLA fields. For the SLA fields, the Cyclonic Eddies (CEs), Anticyclonic Eddies (AEs) and their associated trajectories have a balanced contribution with a ratio of 51 % vs 49 %, whereas for the ADT fields, the CEs outnumber the AEs by 57 % vs 43 %. In both cases, only 25 % of the trajectories last at least 15 days and will be used in this study, but they are composed of 80 % of the individual detected eddies (Table 1).

The lifetime of the selected trajectories is independent of which SSH field was used for the detection, or of the rotating sense. The Mediterranean Sea is favorable to short-living eddies, with half of the trajectories used in our study lasting 15 – 30 days (19 % of the individual eddies). Eddies detected for one to three months represent another third of the trajectories and 35 % of the individual eddies. In contrast, only 8 % of our selected trajectories last between three to six months, and only 4 % last more than six months; the former and the latter are composed respectively by 18 % and 32 % of the individual eddies. The very long-lived eddies (lifetimes > 2,5 years) are more likely anticyclones than cyclones in both the SLA (23 AEs and 9 CEs) and the ADT (28 AEs and 12 CEs). The small number of main trajectories that last more than 3 months should be kept in mind throughout this article.

4. Results

4.1. Surface characteristics of the detected eddies

We present here the temporal evolution of the radius, amplitude and eddy kinetic energy associated with different lifetime eddies detected from the SLA or ADT fields (Figure 3). Eddy lifecycles are composed of three typical stages (a growing phase, a mature phase and a decay phase) that have been observed in various places (Escudier et al., 2016; Fang and

Morrow, 2003; Pegliasco et al., 2015; Samelson et al., 2014) based on SLA-detected eddies. Figure 3 shows the first comparison of these lifetime statistics based on the ADT-detected fields as well.

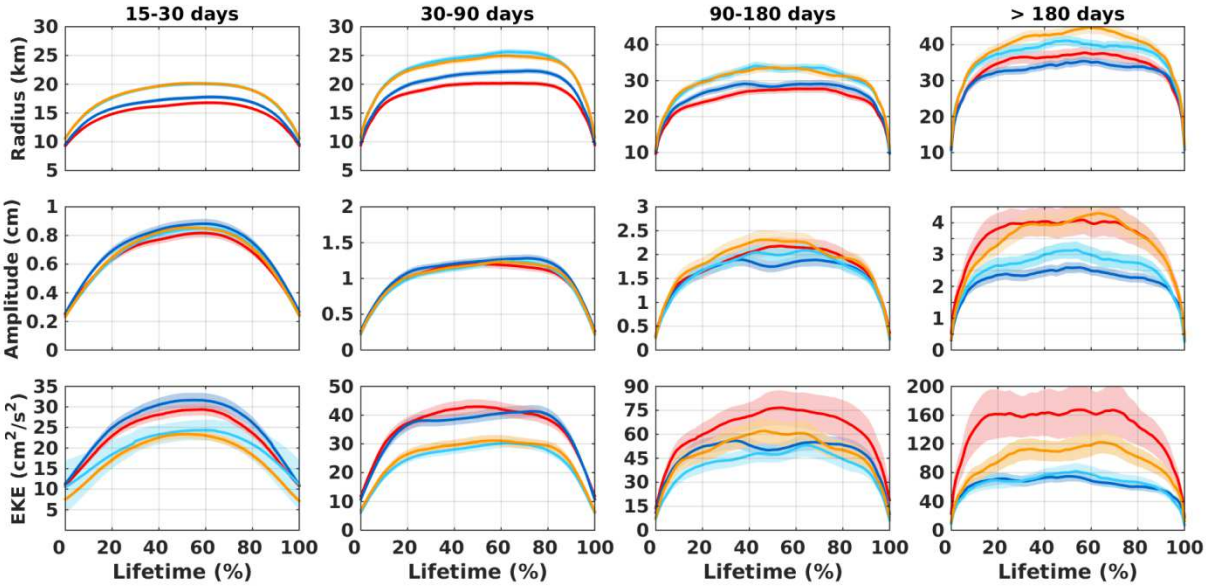

Figure 3 : *Mean temporal evolution (solid lines) and associated student errors (shadings) of Radius (top), Amplitude (middle) and EKE (bottom) for main trajectories as a function of normalized lifetime. AEs are red in the ADT and orange in the SLA; CEs are blue in the ADT and cyan in SLA.*

Firstly, the SLA-detected eddies show similar lifetime evolutions as those from previous studies in the Mediterranean Sea, using slightly different tracking techniques (Escudier et al., 2015, 2016). Our results confirm these previous studies, showing that AEs and CEs detected from SLA fields have similar radii, amplitude or EKE for lifetimes shorter than 3 months. However, for eddies lasting longer than 3 months, AEs tend to have larger radii and amplitudes compared to CEs, with similar larger differences in EKE. The few eddies lasting longer than 6-months (4 % of eddies) occur mainly in the Western Alboran Gyre, the Algerian Current region, the Pelops Eddy region South of Greece, the Ierepetra region south of Crete and the Levantine basin, regions dominated by deep-reaching energetic AEs.

Figure 3 also clearly indicates how the eddies detected in the ADT fields or the SLA fields have different mean characteristics over their lifetimes in the Mediterranean Sea. The SLA-detected eddies have larger radius than the ADT-detected eddies by 3 – 8 km during their mature phase (~15 % of the radius of the SLA-detected eddies) (Figure 3, top). On the other hand, the amplitudes of the ADT or SLA-detected eddies during their mature phase are quite similar (0.8 cm for the 15 – 30 days lasting trajectories, 1.15 cm for the 30 – 90 days lasting trajectories) (Figure 3, middle), and eddies lasting longer than 3 months have slightly higher amplitudes in the SLA fields than in the ADT fields. The EKE of the AEs detected in the ADT fields are consistently higher than the AE EKE in the SLA fields, although the longest-lived CEs have the same EKE in both the SLA and ADT fields.

The reason why the SLA-detected radii are larger than the ADT-detected radii may be due to the joint presence of eddies and meanders in these fields, and the way our eddy detection technique searches for the largest closed contour from either type of anomaly. In the SLA fields, both eddies and meanders can be "anomalies" from the mean and it is easier to form a large closed contour just inside a large meander. On the other hand, the ADT fields include the additional mean circulation around recurrent meanders, forcing the main contours to be open, and the first closed contour will be located further inside the meander, with a smaller radius.

Since the ADT-detected eddies have a smaller radius, their EKE (calculated as the mean value within the eddy contour) tends to be larger than the equivalent SLA-detected eddy. The ADT mean EKE values will extend out to the region of maximum velocities around the eddies, whereas the SLA eddies having a larger radius, will be including more points on the edge of the eddy with a weaker velocity.

For eddies lasting longer than 3 months, these differences in the radii, amplitude and EKE are more pronounced (Figure 3). Given the small number of these long-living eddies,

these statistics are dominated by a few geographical sites, which are investigated in the next section.

4.2. ADT- and SLA-detected eddies frequency

There are large geographical variations in the detection of eddies based on the SLA or ADT fields which are hidden in the mean statistics in Figure 3. This strong geographical difference between the use of the SLA or the ADT for the eddy detection appears on the frequency maps (Figure 4), showing the percentage of time that each grid point has spent within an AE or a CE, or outside of an eddy. The grid step is 0.25° in longitude and latitude.

Grid points are more often located outside eddies in the ADT field compared to the SLA (Figure 4a,d, light colors), mostly due to the higher number of individual eddies detected in the SLA (Table 1) and their larger radius (Figure 3). Eddies are not well detected in the coastal band in either field, likely due to the difficulty in obtaining good altimetry data near the coast (Dibarboure et al., 2011; Escudier et al., 2013; Pujol and Larnicol, 2005). This "eddy-free" coastal zone extends further offshore in the ADT field (~60 km) than in the SLA (~25 km). An explanation may be due to the difficulty in closing contours in the meandering alongshore currents contained in the ADT maps, whereas in the SLA, moving meanders clearly appear as a closed contour because it is an anomaly compared to the mean circulation.

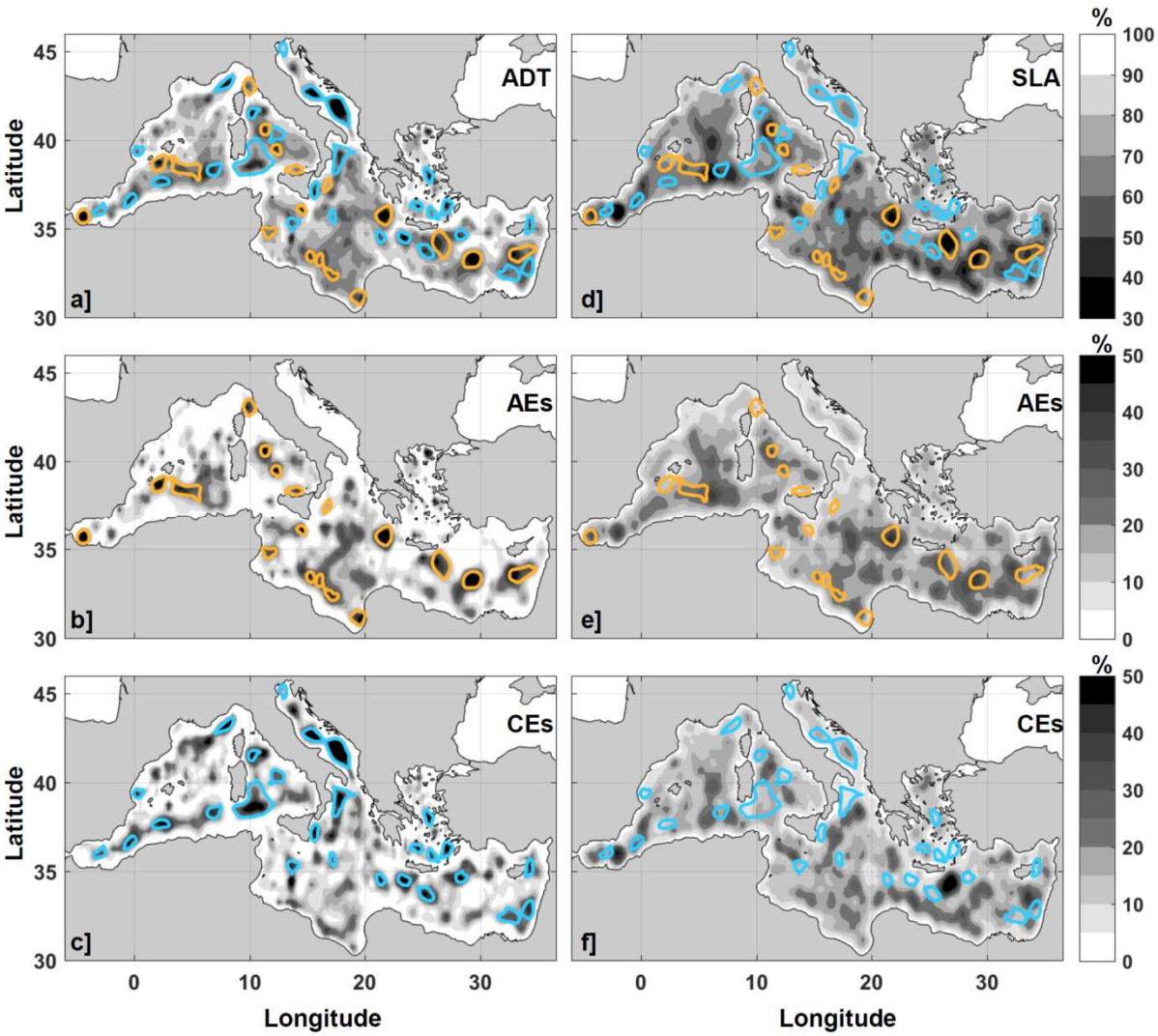

Figure 4 : *Percentage of time spent by each pixel of 0.25°x0.25° outside eddies for* **a]** *the ADT and* **d]** *the SLA, within an Anticyclonic Eddy for the* **b]** *ADT and* **e]** *the SLA, and within a Cyclonic Eddy for* **c]** *the ADT and* **f]** *the SLA . Dark tones depict a high occurrence of eddies, white tones highlight areas free of eddies. The MDT closed circulations contours are highlighted in orange for anticyclonic and in light blue for cyclonic.*

The frequency of occurrence of AEs and CEs from the ADT detection fits very well with the closed MDT contours, highlighted in orange for anticyclonic circulations (Figure 4b) and in light blue for cyclonic circulations (Figure 4c). The longest times of AEs detected in the ADT match the main well-known anticyclonic features (e.g. the Alboran Gyres, the Capraia, Pelops, Ierapetra, Marsa-Matruh and Shikmona Eddies, see Figure 2) and the highest

parts of the MDT (South of the Balearic Islands, in the Gulf of Syrte off the northern coast of Libya, and in the center of the Tyrrhenian Sea) (Figure 4b). The opposite occurs for the CEs detected in the ADT : the lowest percent of time corresponding to the previously listed anticyclonic features (Figure 4c). As expected, the strong cyclonic features visible in the MDT are "free of AEs" but full of CEs, as the Western Cretan Eddy, the Rhodes Gyre, almost all the Adriatic Sea, the cyclonic Bonifacio Eddy (10°E, 41.5°N) and the cyclonic pattern North off Tunis (7°E, 38.3°N).

The frequency maps are quite different for the SLA detected eddies (Figure 4e,f). Firstly, in regions of low and high MDT, and in the coastal regions free of ADT-detected eddies, SLA-detected eddies exhibit a low frequency of occurrence but are not absent. Some anticyclonic regions described in the ADT are also anticyclonic in the SLA (i.e. the Alboran Gyres, the anticyclone part of the Bonifacio Dipole, the Pelops, Ierapetra, and Mersa-Matruh Eddies), reflecting the strengthening of these eddies compared to their mean state. Areas such as the Gulf of Syrte, the Gulf of Gabès (off the western Tunisain coast), the region North of Sicily, in the northern part of the Ionian basin or to the South of the Balearic Islands, exhibit low SLA-detected eddies frequency, whereas the same places show high ADT-detected AEs frequencies. As the SLA reflects variations around a mean state, areas of low SLA frequency and high ADT frequency generally characterize stable and recurrent AEs.

An anticyclonic pattern is visible in the SLA between Cyprus and Syria (~35°E, 35°N), whereas only CEs were detected in the ADT in this area. Similarly in the Algerian basin around ~7°E, 38°N, AEs are present in the SLA whereas the area is occupied by CEs in the ADT. Whereas, CEs in the SLA can be present at typical anticyclonic locations, such as the Eastern Alboran Gyre, the Ierapetra and the Shikmona Eddies (Figure 4f). These situations could indicate weakening, absence or reversal of the mean circulation.

Some AEs and CEs are detected in the SLA on the Eastern and Western fringes of the MDT closed circulations. These shifted positions of the cyclonic and anticyclonic eddies in the SLA may be due to the local displacement of a strong pattern present in the MDT.

In general, the ADT anticyclonic and cyclonic frequencies follow the closed contours of the MDT, whereas in the SLA, the eddies are more homogeneously distributed.

4.3. Generation, lifetime, propagation

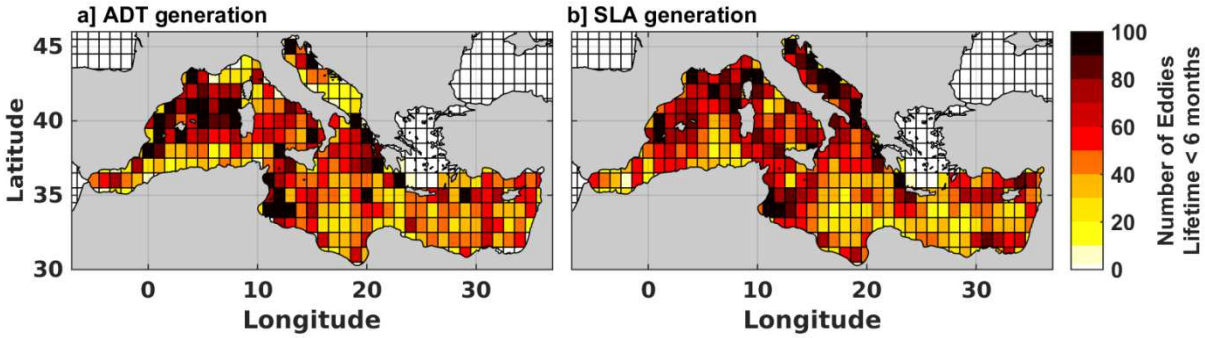

Figure 5 : *Number of trajectories lasting less than 6 months generated in 1°x1° boxes for* **a]** *ADT and* **b]** *SLA.*

Figure 5 summarizes the spatial distribution of the generation areas for both the ADT and the SLA for trajectories lasting less than 6 months while Figure 6 presents the generation position of the 4% of longer trajectories lasting more than 6 months. In the SLA, numerous short-lived AEs and CEs are generated in the Gulf of Gabès (off the eastern Tunisian coast) and in the Adriatic Sea (Figure 5b). In the ADT, the Adriatic Sea is mostly occupied by very long-lived CEs (Figure 6b) and the Gulf of Gabès generates 6 to 12 months AEs (Figure 6a) in addition of the short-lived eddies (Figure 5a). These areas are particularly shallow and exhibit closed mean circulations around low and high MDT values (Figure 2), respectively, that favors the persistence of long-lived ADT-detected eddies. The coastal band generates more eddies in the SLA than in the ADT, especially along the Algerian coast and in the northern part of the Liguro-Provençal Basin, both AEs and CEs (Figure 5). The small number

of eddies generated in these regions is not surprising, since the frequency of AEs and CEs occurrence are very low close to the coastline (Figure 4b,c). The Liguro-Provençal Basin is thus occupied only by very long-lived CEs in the ADT fields (Figure 6b).

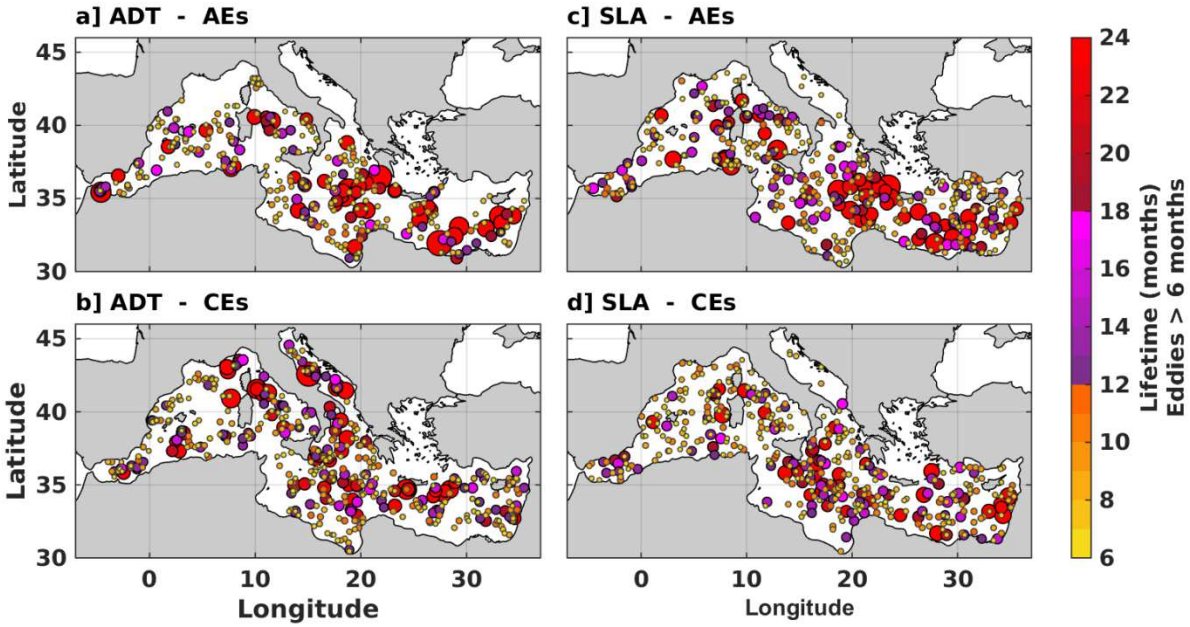

Figure 6 : *Lifetime of the main and merged trajectories lasting longer than 6 months, plotted at the first position of the centers, for* **a,b]** *AEs and CEs in the ADT, and* **c,d]** *AEs and CEs in the SLA. More than one trajectory can be generated at the same location. The size of the points is also a lifetime indicator (larger disks for longer trajectories).*

Contrary to the short-lived eddies generated almost homogeneously in each basin (Figure 5), the long-lived eddies lasting more than 6 months are generated in more specific places, typically in the centers of the basins and in the well identified permanent closed circulations (Figure 6). In both the SLA and ADT fields, the long-lived AE trajectories start at the location of the Western Alboran Gyre, the anticyclonic part of the Bonifacio Dipole, the Pelops, Ierapetra, Mersa-Matruh and Shikmona Eddies typical positions. In contrast, the CE trajectories are mostly generated in the Northern Liguro-Provençal Basin, the Adriatic Sea, and at the location of the Western Cretan Eddy, in the Rhodes Gyre and along the easternmost coast. This distribution is closely linked to the frequency maps of Figure 4, with again a clear

separation between AEs and CEs following the MDT patterns for the ADT-detected eddies, and a more homogeneous SLA-detected eddies distribution.

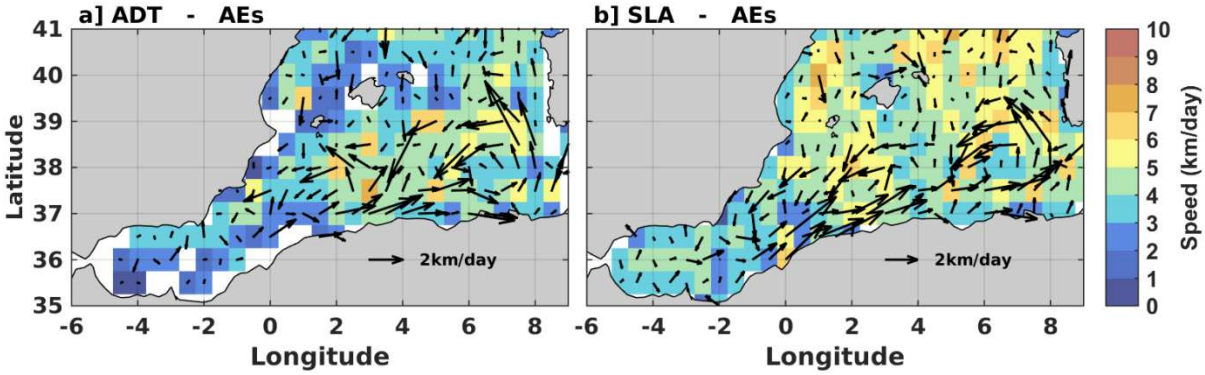

Figure 7 : Propagation speed (shading, km/day) and mean direction (arrows) for the AEs detected in **a]** *the ADT and* **b]** *the SLA. No information are given if fewer than 25 eddies were detected in a 0.5 x 0.5 grid cell.*

The dissipation areas are similar to the generation zones, both for the ADT- and the SLA-detected eddies (not shown). This is due to the small displacement of the eddies during their short lifetimes. On average, Mediterranean eddies have a weak propagation speed of 3 – 5.5 km/day (~3.5 – 5.5 cm/s), similar to those estimated in previous studies (Escudier et al., 2016; Hamad et al., 2006; Mkhinini et al., 2014; Sutyrin et al., 2009). The only clear circulation pattern observed for the eddies' displacement occurs in the Algerian basin, where the AEs follow two cyclonic paths centered at 2°E and 7°E, in both the ADT and the SLA fields (Figure 7) (Escudier et al., 2016; Font et al., 2004; Isern-Fontanet et al., 2006; Pessini et al., 2018; Puillat et al., 2002; Testor et al., 2005). Apart from this specific region, the speed arrows are small, meaning that the eddies tend to move without a preferential path over long distances, and are mostly stationary over long periods.

4.4. Collocating eddies detected on the two SSH fields

The contrast in frequency maps and certain physical characteristics, in particular the radius, lead us to investigate the characteristics of the eddies present in both the ADT and the SLA, or absent in one dataset. The comparison between the ADT- and the SLA-detected eddies and *vice versa* is performed map by map, searching for an intersection between the eddies' contours detected within two SSH fields. Note that this analysis is performed for the detected eddies lasting more than 15 days in the first SSH field (ADT or SLA); the corresponding eddies are sought in the second SSH field (SLA or ADT) regardless of their trajectories' lifespan. The second SSH field may not contain a corresponding eddy, or may have one or more intersections with the initial contour. A collocated area is then computed as a percentage of the overlapping area between the eddies in the two SSH fields, with respect to the area of the eddy in the initial dataset. In the case of multiple intersections, eddies are classified from the largest to the smallest overlapping area. Then, the rotation sense of the collocated eddies is compared with the initial eddy, and noted as "same" or "different" (Table 2). We consider that the rotation is conserved if at least one collocated eddy has the same sense as the initial one, whereas the rotation is different when all the collocated eddies have a different rotating sense.

4.4.1. Quantitative comparison between the two datasets

We recall that we detect more eddies in the SLA fields than in the ADT fields, in particular for AEs (Table 1). Indeed, 18 % of AEs detected in the ADT have no collocated eddies in the SLA fields (~21 % for the CEs), whereas 30 % of AEs detected in the SLA have no collocated eddies in the ADT (~25 % for the CEs; Table 2). For the ADT-detected eddies, 80 % of the AEs and 76 % of the CEs have a collocated eddy in the SLA fields with the same rotation, and only a few cases (~3 %) are associated with an opposite rotating eddy. When starting from the more numerous eddies in the SLA field, AEs have fewer collocations with

AEs in the ADT (~67 %) but AEs have slightly more collocations with CEs (~4 %). CEs detected in the SLA have a higher collocation with CEs in the ADT (~74 %), and the lowest collocation with the opposite rotating eddies, for only 1.3 % of the eddies.

		No intersection	**Same**	**Opposite**
ADT → SLA	**AEs**	64658 (17.7 %)	291077 (79.8 %)	9000 (2.5 %)
	CEs	98138 (21.2 %)	349278 (75.6 %)	14777 (3.2 %)
SLA → ADT	**AEs**	130541 (29.6 %)	294288 (66.8 %)	15922 (3.6 %)
	CEs	113937 (24.5 %)	344735 (74.2 %)	5906 (1.3 %)

Table 2: Number and percentage of ADT- and SLA-detected eddies with no intersections with eddies in the other product, at least one intersection with an eddy rotating in the same sense (Same), and with intersections only with eddies rotating in opposite sense (Opposite), for all lifetimes.

This statistical comparison shows that whether we use the ADT or SLA maps, the majority of AEs and CEs are collocated between 65 % and 80 % of the time; between 20 % and 30 % of eddies are detected in one field but not in the other ; and only a few percent (1 – 4 %) of eddies have an opposite rotation.

We have also analysed how the radius, amplitude and EKE of the different eddies vary, depending on whether they are collocated in the ADT or SLA fields or not. Whatever product is used, the less energetic and smallest eddies ($R < 15$ km) are more likely to have an opposite rotation or absence of collocation in the other field, whereas the more energetic and larger eddies ($R > 15$ km) are more likely to be collocated properly with the same rotating eddy type (not shown). So a large and intense eddy with a clear SSH signature will be correctly identified in both the SLA and the ADT, while small eddies close to the Rossby radius are not fully captured by either altimetric field.

Some of the detected eddies with a small radius (R < 15 km) have some reliability if they are present in the two datasets and propagate for more than 15 days. Indeed, these eddies may be even more energetic in reality, since the filtering and the optimal interpolation steps in the processing of the altimetry gridded mapping smooth out the small scales (Dibarboure et al., 2011; Morrow et al., 2017, 2018; Morrow and Le Traon, 2012; Pascual et al., 2013; Pujol et al., 2016).

4.4.2. Geographical distribution of same and wrong collocations:

The location of the detected eddies that have a reverse rotation sense in the ADT and SLA products (1 – 4 %, see Table 2) is shown in Figure 8a,c for AEs. These reverse rotation cases are mainly observed in regions where the MDT is strong and/or the eddies are small and weak. For the SLA-detected AEs, the regions with opposite rotating eddies are the Liguro-Provençal Basin, the Adriatic Sea, the Sardinia Chanel, the Western Cretan Eddy and the Rhodes Gyre (Figure 8c). These sites are characterized by strong cyclonic circulation in the MDT and very few closed contours were detected in the ADT (Figure 4c). The western part of the Algerian Current also shows mismatches with the SLA -detected AEs. In this region, there are fewer ADT-detected AEs and more CEs (Figure 4b,c) and so more mismatched eddies with a reverse rotation (Figure 8a). The Western Alboran Gyre, the Capraia and the Ierapetra Eddies are regions with the most mismatches for the ADT-detected AEs, due to the presence of numerous CEs detected in the SLA fields there. The Balearic Island region also exhibits high rates of mismatches, since the topography complicates the presence of closed SSH contours.

Figure 8 shows that all of the regions where AEs and CEs were present in the ADT field, with a high eddy frequency (Figure 4b,c), have a good match with the SLA-detected eddies (Figure 8b,d, dark tones). Only the Liguro-Provençal Basin, the Western Cretan Eddy and the Adriatic Sea have no collocation for the AEs due to the absence of AEs detected there

on the ADT fields ; similarly, for the Western Alboran Gyre for the CEs. Again, we note the few ADT-detected AEs matching SLA-detected AEs in the southern part of the Algerian Basin (Figure 8b). This is due to the low number of AEs detected there in the ADT fields, as in this region the Algerian current is often meandering with no closed contours, before a possible eddy formation offshore (Millot, 1985; Obaton et al., 2000; Pessini et al., 2018; Puillat et al., 2002; Salas et al., 2002; Salas, 2003; Taupier-Letage, 2003).

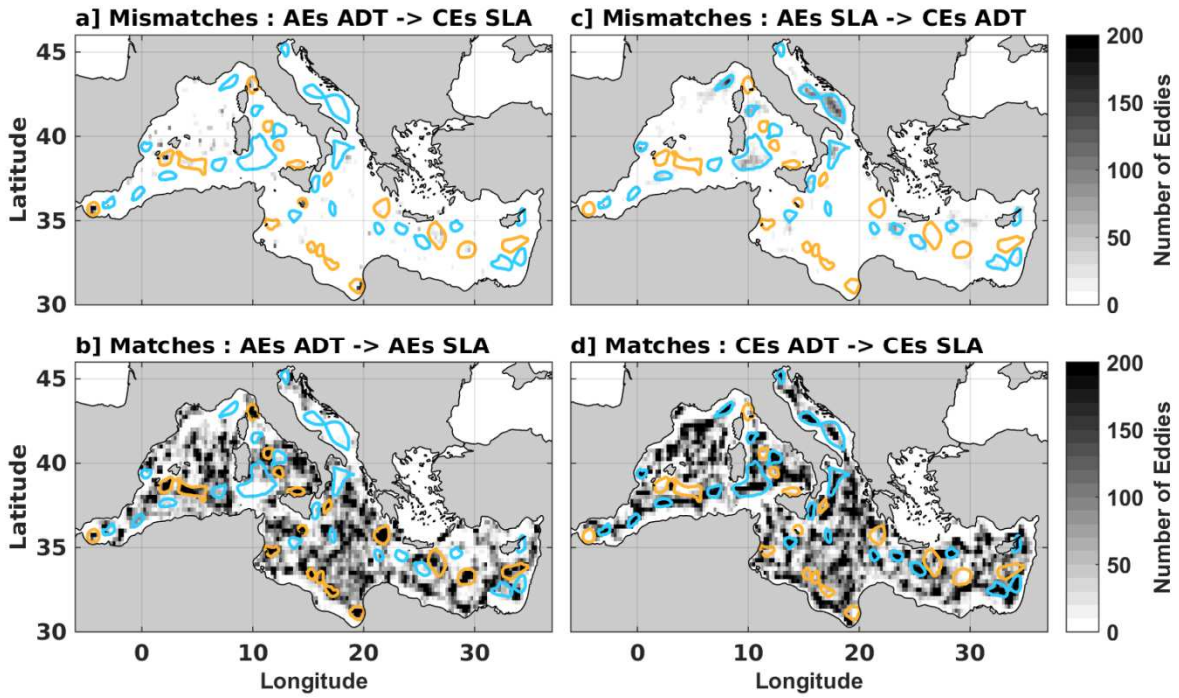

Figure 8 : Number of eddies in 0.25°x0.25° boxes (in gray shades) having an opposite rotating sense in the two SSH fields: **a]** *AEs in the ADT corresponding to CEs in the SLA,* **c]** *AEs in the SLA corresponding to CEs in the ADT; and having the same rotating sense:* **b]** *AEs in both the ADT and the SLA,* **d]** *CEs in both the ADT and the SLA. The MDT closed circulations contours are highlighted in orange for anticyclonic and in light blue for cyclonic.*

Globally, there is a larger area of collocation when starting from ADT to SLA (on average, ~70 % for the AEs, ~60 % for the CEs) than from SLA to ADT (50 % on average for both AEs and CEs) (not shown). The ADT-detected eddies are generally smaller and occur within the contours of the SLA-detected ones for the same feature. Mismatches appear

preferentially in the case of small structures, although even large structures can have opposite rotations in the ADT and SLA fields, such as the Ierapetra Eddy.

4.5. The Ierapetra case

	ADT	**SLA**
Only AEs centers	2475 (43 %)	1399 (24 %)
Only CEs centers	990 (17 %)	3394 (59 %)
Both AEs and CEs centers	131 (3 %)	136 (3 %)
No eddy center	2137 (37 %)	804 (14 %)

Table 3: Number and percentage of daily SSH maps where eddies' centers (AEs or CEs) are detected or not in each SSH field in the box [26 – 27°E; 33.75 – 34.65°N]. The total number of maps is 5733.

The Ierapetra Eddy, located at the south-eastern corner of Crete, is a well known strong, seasonal, recurrent anticyclonic feature, which is present in the MDT (Figure 2). This eddy is mostly anticyclonic in the ADT field, but for the SLA, where the mean circulation has been removed, the Ierapetra Eddy location exhibits both anticyclonic and cyclonic frequencies (Figure 4b,e,f), due to the strengthening or weakening of the eddy, or a shift in its position. Thus, the Ierapetra Eddy is a relevant example of the difficulty in interpreting the sea level anomalies in regions where intense recurrent or quasi-permanent structures are present.

We have quantified the occurrence of an AE or CE center for both the ADT and the SLA fields, within the main zone encompassing the MDT Ierapetra Eddy signature [26-27°E; 33.75-34.65°N] named after *Ierapetra zone* (Figure 9, black box). Within this Ierapetra zone, 43 % of the time there is an AE center in the ADT, and only 17 % of the time a CE center; whereas for the SLA, the presence of AEs and CEs are completely different : an AE center is

present for 24 % of the time, and a CE center for 59 % of the time (Table 3 and Figure 4). There are no eddies present in the zone 14 % of the time in the SLA, contrary to the ADT where the zone is free of eddies 37 % of the time.

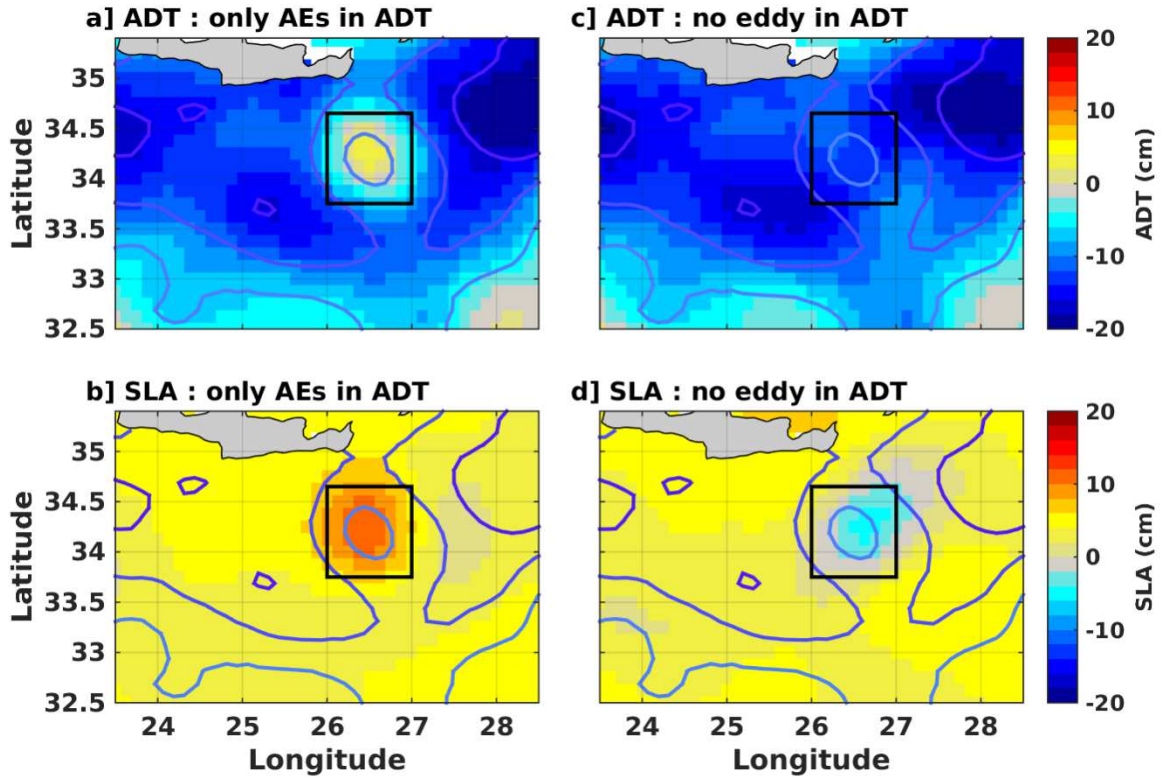

Figure 9 *: Composite ADT* (**a,c**) *or SLA* (**b,d**) *field (in cm) when* **a,b]** *only AEs centers are detected in the ADT field within the box* [26 – 27°E; 33.75 – 34.65°N]*;* ***c,d]*** *no eddy centers are detected within the box in the ADT field. The contours are the MDT every 5 cm (see Figure 2 for the values).*

To understand why we have such differences, we have constructed composite ADT and SLA fields for the time periods when AEs centers are detected in the Ierapetra zone in the ADT field, and when no centers are present in the ADT field (Figure 9).

As expected, when AEs centers are detected in the ADT, the composite SLA and ADT fields both show an anticyclonic signature (Figure 9a,b), with amplitudes of ~8 cm. When no center is present in the ADT, there is no cyclonic nor anticyclonic pattern in the ADT

composite (Figure 9c) whereas in the SLA composite, a clear cyclonic feature is visible (Figure 9d), also with an amplitude of ~8 cm. Since the Ierapetra Eddy is a recurrent feature, part of its signal is contained in the MDT (Figure 2). Thus the absence of the Ierapetra Eddy, due to no formation or to its displacement, leads to a negative SLA, e.g. a cyclonic pattern by construction (Isern-Fontanet et al., 2006; Schouten et al., 2003). To our knowledge, no *in situ* data have confirmed the presence of realistic cyclonic eddies at this location.

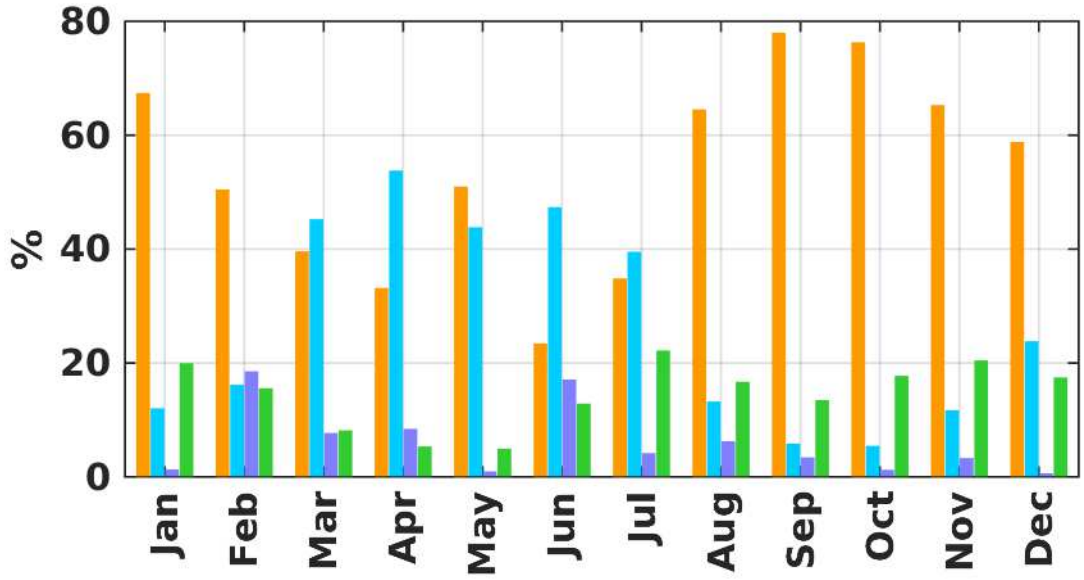

Figure 10 *: Monthly percentage of occurrence of SLA features occuring within an ADT AE in the Ierapetra Eddy zone. Orange is reinforcement (AE in SLA), cyan is weakening (CE in SLA), purple is slight displacement (CE and AE in SLA) and green is no change (no eddy in SLA).*

The differences between ADT- and SLA-detected eddies can provide useful information on the strengthening, weakening, or displacement of eddies. If we considered that the ADT allows a correct detection of the Ierapetra Eddy, we can deduce that an AE detected in both the SLA and the ADT implies a reinforcement of the mean Ierapetra Eddy. We have calculated the seasonal variations of these events (Figure 10). This reinforcement, when an AE is detected in the SLA at the Ierapetra Eddy mean position, occurs between August and

January (Figure 10, orange), in agreement with the observed generation of Ierapetra Eddies (Amitai et al., 2010; Ayoub et al., 1998; Hamad et al., 2006; Ioannou et al., 2017; Mkhinini et al., 2014). In a similar way, when a CE is detected in the SLA field but an AE is present in the ADT, this means that the Ierapetra Eddy is weaker than its average (for more than 40 % of the time between March and July, Figure 10, cyan). No eddies are detected in the SLA field on average for 15 % of the time when an AE is detected in the ADT field (Figure 10, green), corresponding to events where an Ierapetra Eddy is close to its mean signature in the MDT. For 5 % of the time, the Ierapetra Eddy moves slightly from its mean position, leading to the presence of both AE and CE in the SLA.

This example shows that the ADT fields provide a better description of the Ierapetra Eddy yet by looking at SLA fields (or the ADT minus MDT fields), we also have a good description of the seasonal variations in the eddy's reinforcement or weakening. However, with the SLA fields alone, it is difficult to distinguish the absence, the spatial shift or the amplitude changes of a geographically recurrent eddy.

5. Discussion

Our study has concentrated on comparing the two ADT and SLA altimetric products using our chosen closed contours eddy detection and tracking technique. Before we address the dynamics of the different regional eddies, we will discuss how the quality of our detected eddies will depend on three components: (*i*) the resolution and accuracy of the altimetric gridded SSH maps; (*ii*) the MDT used in our analysis; (*iii*) our eddy detection and tracking schemes.

In section 3.1, we stated that the effective resolution of the SSH fields is on average 100 km in wavelength (Pascual et al., 2013), or 25 km in eddy radius. This is based on long time series and basin-wide statistics, yet smaller eddies still exist in the gridded maps. As no

threshold was applied for the eddy detection, these small eddies constituting the growth and the decay of a trajectory can be below the average spatial resolution of the regional altimetric product. The presence of such small eddies at every start and end of trajectories suggests that they may be real (see Figure 3), although they may not be observed at all places and all times by altimetry. Any gain in resolution in altimetry data is thus crucial to properly describe a large part of the mesoscale activity in the Mediterranean Sea (Amores et al., 2018; Durand et al., 2010; Pujol et al., 2012). The future wide-swath altimeter mission SWOT should contribute greatly to increasing the spatial resolution of altimetric observations after 2021.

The quality of all of the ADT detected eddies also depends on the robustness of the MDT. This version of the 2014 MDT has improved shorter-scale structures in the Mediterranean Sea compared to previous versions, based on validation with independent *in situ* data (Rio et al., 2014). Even so, the MDT does not correctly resolve all of the smaller coastal or mesoscale mean circulation features. For example, the spatial distribution of the *in situ* data used in the MDT is not homogeneous: large areas have few hydrological profiles and drifters to constrain the MDT (see Figure 3 and 4 of Rio et al., 2014). In these regions with few *in situ* observations, the MDT may not be a good representation of the mean and will therefore introduce errors in the ADT eddy detection. In addition, since the geoid is not accurate enough at small scales, the first guess of the MDT is determined based on an ocean circulation model, which has its own errors. Furthermore, the correlation scales for the MDT analysis are based on functions developed for the North Atlantic (Arhan and Colin de Verdière, 1985), and are thus not fully adapted to the specificities of the Mediterranean Sea. Finally, the validation of the MDT was made with a limited number of independent drifters, hydrological profiles and surface temperature, but these are not available consistently over the whole Mediterranean Sea. All of these points lead to uncertainties in the small-scale MDT structures, that directly impact on the quality of the ADT fields, and the eddies detected with

these fields. In the future, we expect a big improvement in the MSS, marine geoid and thus the MDT fields after the first years of the SWOT mission, but not before 2024.

Taking into account these caveats on today's products and eddy detection, the differences we find between eddies detected in the SLA and the ADT products can help us identify where the eddy-detection methodology is well suited to the local dynamics. We can characterize different situations where the SLA and the ADT strongly differ in terms of eddy detection:

- in the coastal areas of the Western Mediterranean Sea, where the Algerian Current and the Northern Current flow;

- in the recurrent closed gyre circulations, with a strong signature in the MDT, such as the Western Alboran Gyre, the Adriatic Sea, the Liguro-Provençal and the Rhodes Gyres;

- in geographically recurrent mesoscale features which have an imprint in the MDT, such as the Ierapetra Eddy.

The Algerian Current is known for its large meanders – which eventually detach from the current and become energetic anticyclonic eddies. This situation is not well captured in either the ADT or the SLA products. When an alongshore current is meandering, the meander will appear as a closed contour near the coast in the SLA field, whereas in the ADT the contour will be closed only if the meander contains an eddy. This is the case of M1 presented in Figure 11, where the Algerian Current is strongly deflected offshore between 1 – 2 °E in an anticyclonic meander. This meander is represented in the SLA as a strong positive anomaly, whose dimensions allow the detection of a closed contour.

In the ADT field, a closed contour near the coast appears only if the whole jet is deflected far offshore by the meander (e.g. 37°N, 8°E, M2 in Figure 11). Small closed contours can be detected in the ADT at the core of the meanders, but as our tracking method

is based on the overlapping of eddy contours from one day to another, their size is often too small and their displacement is too fast to properly capture them. For the Algerian Current, whose mean position is located close to the coast in the MDT (Figure 2), the SLA fields detect a series of eddies rather than meanders of the current from ~0°E to ~8°E, whether the eddies are embedded in the meanders or not. The meander M1 formed at 2°E in Figure 11 will grow enough to become a detected eddy in both fields around 4°E, but the contour is too small in the ADT to be attached to a trajectory. In contrast, any Algerian Eddies detected in the ADT tend to be fully developed although their alongshore buildup is missing, particularly between ~0 – 4°E. So, neither of the products are correctly detecting the closed-contours eddy evolution here.

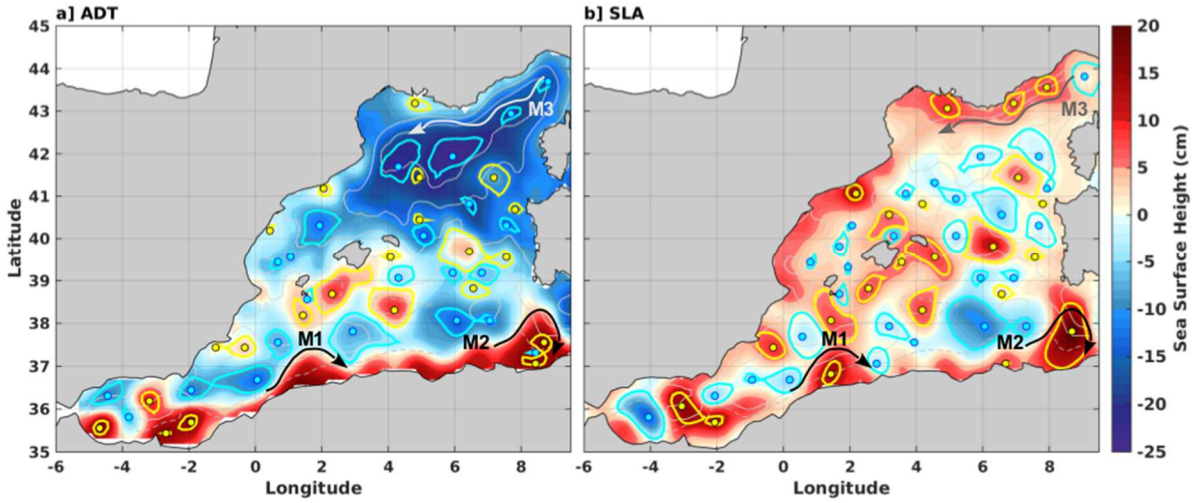

Figure 11 *: Snapshot of the eddies detected on the 15 Janvier 2003 in a] the ADT and b] the SLA. The yellow contours and points are for AEs, cyan are for CEs. M1, M2 and M3 are three meanders identified in ADT field and reproduced in the SLA field.*

The Northern Current in the Liguro-Provençal Basin is another example of a coastal and meandering current but, in contrast to the Algerian Current, its small meanders do not develop into large eddies that can be detected and tracked by altimetry maps. When the alongshore current detaches from the coast, anticyclonic closed contours are present in the

SLA field, whereas in the ADT the anticyclonic meanders can be seen but are never closed (Figure 11, M3). These meanders vary in amplitude and position from the mean state of the current, and are detected as closed contours in the SLA field and falsely represented as eddies.

In both of these examples, the closed-contour eddy detection applied to the ADT maps will only detect the large eddies and cannot detect any changes in amplitude or movement of the meandering current, nor the smaller eddy formation processes. For the SLA detected eddies, local knowledge of the characteristics of the coastal situation is essential to differentiate between variations in the meanders and position of the Northern Current, or the moving meanders and eddies of the Algerian Current, since they will appear similarly in our SLA eddy detection and tracking.

The mean circulation in the Mediterranean Sea often contains closed contours with the same amplitude and horizontal extent as the mesoscale eddies. When the MDT shows high values, it becomes difficult to close a contour associated with a circulation of the opposite rotation in the ADT, as it would imply a strong reversal of the mean circulation. This explain why only AEs (CEs, respectively) can be detected in closed anticyclonic (cyclonic) MDT circulations in the ADT maps. For the SLA fields, the absence of a recurrent feature having an imprint in the MDT will be visible in the SLA as a closed contour with an opposite rotation compared to the mean circulation, as for the case of the Ierapetra Eddy. The SLA field is associated with geostrophic velocity anomalies, and in these cases, the anomalies should be interpreted as the accelerations and decelerations of the mean flow rather than absolute AEs or CEs. For a cyclonic gyre, a reinforcement of the boundary currents will appear as a cyclonic eddy in the SLA at the gyre location, as in the Liguro-Provençal Basin or in the Adriatic Sea. But when the same cyclonic gyre slows down, an anticyclonic feature will appear in the SLA. The reverse occurs for anticyclonic mean gyres.

This is the case for the **Alboran Gyres.** The Western Alboran Gyre is the most intense, whereas the Eastern one shows more variability (Heburn and La Violette, 1990; Viúdez and Tintoré, 1995). In the ADT field, only AEs are detected in the two gyres, following the positive MDT contours. In the SLA, both AEs and CEs are detected, as a decrease of the mean anticyclonic circulation generates cyclonic anomalies, and its reinforcement leads to anticyclonic ones. The same appears in the Adriatic Sea, where two cyclonic gyres are constrained by the coastline with very low values in the MDT. This leads to the detection of only long-lived CEs in the ADT, corresponding to this mean cyclonic circulation. In the SLA, we can assume that AEs will be associated with a decrease in intensity of the cyclonic mean circulation, whereas CEs reflect an intensification. Moreover, when the circulation is equal to its mean value and position, no eddies will be detected in the SLA. This situation also occurs in the Liguro-Provençal and the Rhodes Gyres, with the added complexity in both cases of a meandering part on their southern edges. For these gyres, the SLA detected eddies will reflect the intensity variations of the cyclonic mean circulation but also the displacement of their southern edges from their mean location.

This difference in the interpretation of a meandering coastal current or a closed mean circulation for both altimetric fields lead us to propose an explanation for the different circulation patterns described in the literature for the feature named the **Latakia Eddy**, located East of Cyprus, offshore of Syria. It is sometimes schematized as a strong anticyclonic meander of the northward alongshore current off Syria (Gerin et al., 2009; Hamad et al., 2006, 2005). Yet Menna et al. (2012) observed with drifters the alternation of a cyclonic circulation with an anticyclonic recirculation is this area. Figure 2 shows a low MDT value here, an imprint of a cyclonic feature, which corresponds with the description of Robinson et al. (1991), based on the POEM (Physical Oceanography of the Eastern Mediterranean) cruises. How do we clarify what is the true circulation there? When eddy detection is made using the

ADT fields, the cyclonic pattern within the MDT close to Cyprus is negative and it requires a strong reversal to close an anticyclonic circulation, so only cyclones are detected there (Figure 4c). The mean situation of the eddy detection can thus be interpreted as the recurrent presence of a cyclonic eddy, as confirmed by the Robinson et al. (2001) description. When the detection is made with the SLA fields, the anticyclonic meanders generated by the northward current off Israel and Syria or the decrease of the cyclonic circulation off Cyprus can both lead to closed anticyclonic circulations. A strengthening of the cyclonic circulation off Cyprus is shown as cyclonic eddies in the SLA. Drifters pathways off Cyprus described in Gerin et al. (2009) are anticyclonic, and correspond to a large AE in the SLA, associated in the ADT with a large meander covering the whole cyclonic mean structure. Menna et al. (2012) drifter results are also concordant with our SLA and ADT detection. They show a CE detected in both the SLA and the ADT fields during the cyclonic path of the drifters (thus the cyclonic circulation was more intense than the mean situation). We can reconcile the observed alternation of cyclonic and anticyclonic circulations in the area using the SLA field. So, the terminology of Latakia Eddy may not be the most appropriate to describe the mesoscale activity in this region. Moreover, in this region, there is a large difference in the MDT between the first guess obtained from the geoid model, and the final version improved with hydrological profiles and drifters (Rio et al., 2014). There are only few *in situ* data here to constrain the MDT, and due to the variability of the region, this may impact the final MDT, and thus the ADT, by overestimating the amplitude of the cyclonic mean circulation. The presence of the Cyprus Island is also another difficulty to integrate in the MDT, as it sharp coastal topography is just at the position of the cyclonic mean circulation.

The **Pelops, Ierapetra, Mersa-Matruh and Shikmona Eddies** are four closed anticyclonic circulations, intense and recurrent enough to have their imprint in the MDT. Nevertheless, as we showed for the Ierapetra Eddy, these features are some years not

generated, and sometimes shifted from their mean location. When this happens, a strong cyclonic circulation appears in the SLA at the usual position of these AEs, with a strong anomaly if their signature in the MDT is strong. AEs will be detected if the eddy is at its MDT location and more intense than usual, and no eddy will be detected if it is present at its location and with the same amplitude as in the MDT. Thus, the eddy detection based on the SLA field must be used with caution when the MDT exhibits closed circulations with the same dimensions as the studied features.

All of these cases highlight that the mesoscale eddy field in the Mediterranean Sea has very strong geographical constraints. In turn, the MDT does not have large-scale modulations as in the open ocean, but also has distinct geographically-correlated mesoscale features. As such, the ADT-detected large coherent eddies are generally a better representation of the mesoscale dynamics. Finally, a large part of the mesoscale variability in the coastal Mediterranean currents is linked to meandering jets; however, this component is not detected at all in the ADT closed contour eddy-detection methodology. Yet these meanders contribute greatly to the formation process for the separated coherent eddies. This mesoscale variability is revealed by the SLA "eddies", but requires more careful local interpretation to separate the small eddies from the meandering currents. If the interaction between the meandering jets and the coherent eddies is required, then other methodologies could be applied to the ADT maps.

6. Conclusions

This study aimed at comparing the mesoscale eddies detected in two different mapped altimetry fields, the ADT and the SLA. The number and the surface characteristics of these eddies vary according to the SSH field used for the detection, with more detected-eddies from the SLA field, with globally larger radii than in the ADT for similar amplitudes, leading to more energetic eddies detected in the ADT field.

The spatial distribution of the instantaneous eddies is quite different between the SLA and the ADT. Whereas the ADT frequency follows very well the MDT patterns, the SLA frequency is more homogeneous over the whole Mediterranean basin. From a dynamical point of view, the two datasets have the same correlation between highly generative areas and short lifetimes for the shallowest parts of the basin, and less generation and longer lifetimes in the deep central regions. Two anticlockwise circulations are observed for anticyclonic eddies in the Algerian basin, but otherwise, eddies do not have clear preferential pathways, leading to relative steady eddies.

In comparing the SLA and the ADT dataset of detected eddies, ~15 – 30 % of the eddies do not occur in the other field, particularly in shallow areas and in the case of small eddies. When the eddies are present in the two SSH fields, but have a different sense of rotation, the collocated areas are relatively small, and the characteristics are very different. In general, small eddies are mismatched with a larger eddy in the other SSH field. Indeed, a large majority of eddies are detected in the two datasets with the same rotating sense (65 – 80 %) and have also similar characteristics.

The ADT represents the sum of the mean circulation (MDT) and its temporal variability, whereas the SLA is only the variable part of the sea surface. The patterns detected in the SLA fields can thus be linked to different processes such as eddies, meanders, but also the reinforcement, weakening or displacement of the mean jets and recurrent eddy features present in the MDT. In semi-enclosed seas such as the Mediterranean Sea, and in any ocean region with strong geographical patterns, we recommend to study the mesoscale eddies using the ADT fields. However, it is important to keep in mind the limitations of the resolution and accuracy of the altimetric maps as well as of the independent MDT actually constructed from numerical modelling and *in situ* hydrographic data. Yet, altimeter-based SLA fields may be preferable in specific locations where the MDT is not reliable. Moreover, interpreting the

SLA fields requires caution and local knowledge to separate properly the different processes taking place, given the similar intensity, and space and time scales for the mean circulation and the mesoscale eddies.

Acknowledgments: We thank the anonymous reviewers for their constructive comments that greatly improved the manuscript.

Amitai, Y., Lehahn, Y., Lazar, A., Heifetz, E., 2010. Surface circulation of the eastern Mediterranean Levantine basin: Insights from analyzing 14 years of satellite altimetry data. J. Geophys. Res. Oceans 115, C10058. https://doi.org/10.1029/2010JC006147

Amores, A., Jordà, G., Arsouze, T., Le Sommer, J., 2018. Up to What Extent Can We Characterize Ocean Eddies Using Present-Day Gridded Altimetric Products?: J. Geophys. Res. Oceans 123, 7220–7236. https://doi.org/10.1029/2018JC014140

Arhan, M., Colin de Verdière, A., 1985. Dynamics of Eddy Motions in the Eastern North Atlantic. J. Phys. Oceanogr. 15, 153–170. https://doi.org/10.1175/1520-0485(1985)015<0153:DOEMIT>2.0.CO;2

Ayoub, N., Le Traon, P.-Y., De Mey, P., 1998. A description of the Mediterranean surface variable circulation from combined ERS-1 and TOPEX/POSEIDON altimetric data. J. Mar. Syst. 18, 3–40. https://doi.org/10.1016/S0924-7963(98)80004-3

Ballarotta, M., Ubelmann, C., Pujol, M.-I., Taburet, G., Fournier, F., Legeais, J.-F., Faugere, Y., Delepoulle, A., Chelton, D., Dibarboure, G., Picot, N., 2019. On the resolutions of ocean altimetry maps. Ocean Sci. Discuss. 1–27. https://doi.org/10.5194/os-2018-156

Chaigneau, A., Eldin, G., Dewitte, B., 2009. Eddy activity in the four major upwelling systems from satellite altimetry (1992–2007). Prog. Oceanogr. 83, 117–123. https://doi.org/10.1016/j.pocean.2009.07.012

Chaigneau, A., Gizolme, A., Grados, C., 2008. Mesoscale eddies off Peru in altimeter records: Identification algorithms and eddy spatio-temporal patterns. Prog. Oceanogr. 79, 106–119. https://doi.org/10.1016/j.pocean.2008.10.013

Chaigneau, A., Le Texier, M., Eldin, G., Grados, C., Pizarro, O., 2011. Vertical structure of mesoscale eddies in the eastern South Pacific Ocean: A composite analysis from

altimetry and Argo profiling floats. J. Geophys. Res. Oceans 116, C11025. https://doi.org/10.1029/2011JC007134

Chelton, D.B., Schlax, M.G., Samelson, R.M., 2011. Global observations of nonlinear mesoscale eddies. Prog. Oceanogr. 91, 167–216. https://doi.org/10.1016/j.pocean.2011.01.002

Chelton, D.B., Schlax, M.G., Samelson, R.M., de Szoeke, R.A., 2007. Global observations of large oceanic eddies. Geophys. Res. Lett. 34, L15606. https://doi.org/10.1029/2007GL030812

d'Ovidio, F., Isern-Fontanet, J., López, C., Hernández-García, E., García-Ladona, E., 2009. Comparison between Eulerian diagnostics and finite-size Lyapunov exponents computed from altimetry in the Algerian basin. Deep Sea Res. Part Oceanogr. Res. Pap. 56, 15–31. https://doi.org/10.1016/j.dsr.2008.07.014

Damien, P., 2015. Etude de la circulation océanique en Méditerranée Occidentale à l'aide d'un modèle numérique à haute résolution: influence de la submésoéchelle (Study of the oceanic circulation with a high resolution model in the Western Mediterranean Sea : influence of the mesoscale), PhD Thesis. Université de Toulouse, Université Toulouse III-Paul Sabatier.

de Ruijter, W.P.M., Ridderinkhof, H., Lutjeharms, J.R.E., Schouten, M.W., Veth, C., 2002. Observations of the flow in the Mozambique Channel. Geophys. Res. Lett. 29, 140-1-140–3. https://doi.org/10.1029/2001GL013714

Dibarboure, G., Pujol, M.-I., Briol, F., Traon, P.Y.L., Larnicol, G., Picot, N., Mertz, F., Ablain, M., 2011. Jason-2 in DUACS: Updated System Description, First Tandem Results and Impact on Processing and Products. Mar. Geod. 34, 214–241. https://doi.org/10.1080/01490419.2011.584826

Doglioli, A.M., Blanke, B., Speich, S., Lapeyre, G., 2007. Tracking coherent structures in a regional ocean model with wavelet analysis: Application to Cape Basin eddies. J. Geophys. Res. 112, C05043. https://doi.org/10.1029/2006JC003952

Dong, C., Lin, X., Liu, Y., Nencioli, F., Chao, Y., Guan, Y., Chen, D., Dickey, T., McWilliams, J.C., 2012. Three-dimensional oceanic eddy analysis in the Southern California Bight from a numerical product. J. Geophys. Res. Oceans 117, C00H14. https://doi.org/10.1029/2011JC007354

Dong, C., McWilliams, J.C., Liu, Y., Chen, D., 2014. Global heat and salt transports by eddy movement. Nat. Commun. 5, 1–6. https://doi.org/10.1038/ncomms4294

Durand, M., Fu, L.-L., Lettenmaier, D.P., Alsdorf, D.E., Rodriguez, E., Esteban-Fernandez, D., 2010. The Surface Water and Ocean Topography Mission: Observing Terrestrial Surface Water and Oceanic Submesoscale Eddies. Proc. IEEE 98, 766–779. https://doi.org/10.1109/JPROC.2010.2043031

Echevin, V., Crépon, M., Mortier, L., 2003. Simulation and analysis of the mesoscale circulation in the northwestern Mediterranean Sea, in: Annales Geophysicae. pp. 281–297. https://doi.org/10.5194/angeo-21-281-2003

Escudier, R., 2015. Mesoscale eddies in the western Mediterranean Sea : characterization and understanding from satellite observations and model simulations. Grenoble Alpes.

Escudier, R., Bouffard, J., Pascual, A., Poulain, P.-M., Pujol, M.-I., 2013. Improvement of coastal and mesoscale observation from space: Application to the northwestern Mediterranean Sea. Geophys. Res. Lett. 40, 2148–2153. https://doi.org/10.1002/grl.50324

Escudier, R., Renault, L., Pascual, A., Brasseur, P., Chelton, D., Beuvier, J., 2016. Eddy properties in the Western Mediterranean Sea from satellite altimetry and a numerical

simulation. J. Geophys. Res. Oceans 121, 3990–4006. https://doi.org/10.1002/2015JC011371

Fang, F., Morrow, R., 2003. Evolution, movement and decay of warm-core Leeuwin Current eddies. Deep Sea Res. Part II Top. Stud. Oceanogr. 50, 2245–2261. https://doi.org/10.1016/S0967-0645(03)00055-9

Font, J., Isern-Fontanet, J., De Jesus Salas, J., 2004. Tracking a big anticyclonic eddy in the western Mediterranean Sea. Sci. Mar. 68, 331–342. https://doi.org/10.3989/scimar.2004.68n3331

Gerin, R., Poulain, P.-M., Taupier-Letage, I., Millot, C., Ben Ismail, S., Sammari, C., 2009. Surface circulation in the Eastern Mediterranean using drifters (2005–2007). Ocean Sci 5, 559–574. https://doi.org/10.5194/os-5-559-2009

Halo, I., Backeberg, B., Penven, P., Ansorge, I., Reason, C., Ullgren, J.E., 2014. Eddy properties in the Mozambique Channel: A comparison between observations and two numerical ocean circulation models. Deep Sea Res. Part II Top. Stud. Oceanogr. 100, 38–53. https://doi.org/10.1016/j.dsr2.2013.10.015

Hamad, N., Millot, C., Taupier-Letage, I., 2006. The surface circulation in the eastern basin of the Mediterranean Sea. Sci. Mar. 70, 457–503. https://doi.org/10.3989/scimar.2006.70n3457

Hamad, N., Millot, C., Taupier-Letage, I., 2005. A new hypothesis about the surface circulation in the eastern basin of the mediterranean sea. Prog. Oceanogr. 66, 287–298. https://doi.org/10.1016/j.pocean.2005.04.002

Heburn, G.W., La Violette, P.E., 1990. Variations in the structure of the anticyclonic gyres found in the Alboran Sea. J. Geophys. Res. Oceans 95, 1599–1613. https://doi.org/10.1029/JC095iC02p01599

Hecht, A., Pinardi, N., Robinson, A.R., 1988. Currents, Water Masses, Eddies and Jets in the Mediterranean Levantine Basin. J. Phys. Oceanogr. 18, 1320–1353. https://doi.org/10.1175/1520-0485(1988)018<1320:CWMEAJ>2.0.CO;2

Horton, C., Kerling, J., Athey, G., Schmitz, J., Clifford, M., 1994. Airborne expendable bathythermograph surveys of the eastern Mediterranean. J. Geophys. Res. Oceans 99, 9891–9905. https://doi.org/10.1029/94JC00058

Ikeda, M., 1981. Instability and Splitting of Mesoscale Rings using a Two-Layer Quasi-Geostrophic Model on an f-Plane. J. Phys. Oceanogr. 11, 987–998. https://doi.org/10.1175/1520-0485(1981)011<0987:IASOMR>2.0.CO;2

Ioannou, A., Stegner, A., Le Vu, B., Taupier-Letage, I., Speich, S., 2017. Dynamical Evolution of Intense Ierapetra Eddies on a 22 Year Long Period. J. Geophys. Res. Oceans 122, 9276–9298. https://doi.org/10.1002/2017JC013158

Isern-Fontanet, J., García-Ladona, E., Font, J., 2006. Vortices of the Mediterranean Sea: An altimetric perspective. J. Phys. Oceanogr. 36, 87–103. https://doi.org/10.1175/JPO2826.1

Isern-Fontanet, J., García-Ladona, E., Font, J., 2003. Identification of Marine Eddies from Altimetric Maps. J. Atmospheric Ocean. Technol. 20, 772–778. https://doi.org/10.1175/1520-0426(2003)20<772:IOMEFA>2.0.CO;2

Kurian, J., Colas, F., Capet, X., McWilliams, J.C., Chelton, D.B., 2011. Eddy properties in the California Current System. J. Geophys. Res. Oceans 116, C08027. https://doi.org/10.1029/2010JC006895

Laxenaire, R., Speich, S., Blanke, B., Chaigneau, A., Pegliasco, C., Stegner, A., 2018. Anticyclonic Eddies Connecting the Western Boundaries of Indian and Atlantic

Oceans. J. Geophys. Res. Oceans 123, 7651–7677. https://doi.org/10.1029/2018JC014270

Le Vu, B., Stegner, A., Arsouze, T., 2018. Angular Momentum Eddy Detection and Tracking Algorithm (AMEDA) and Its Application to Coastal Eddy Formation. J. Atmospheric Ocean. Technol. 35, 739–762. https://doi.org/10.1175/JTECH-D-17-0010.1

Li, Q.-Y., Sun, L., Lin, S.-F., 2016. GEM: a dynamic tracking model for mesoscale eddies in the ocean. Ocean Sci 12, 1249–1267. https://doi.org/10.5194/os-12-1249-2016

Malanotte-Rizzoli, P., Bergamasco, A., 1989. The circulation of the eastern mediterranean. Part 1. Oceanol. Acta 12, 335–351. https://doi.org/0399-1784/89/04 335 17

Mason, E., Pascual, A., McWilliams, J.C., 2014. A New Sea Surface Height–Based Code for Oceanic Mesoscale Eddy Tracking. J. Atmospheric Ocean. Technol. 31, 1181–1188. https://doi.org/10.1175/JTECH-D-14-00019.1

Matteoda, A.M., Glenn, S.M., 1996. Observations of recurrent mesoscale eddies in the eastern Mediterranean. J. Geophys. Res. Oceans 101, 20687–20709. https://doi.org/10.1029/96JC01111

Menna, M., Poulain, P.-M., Zodiatis, G., Gertman, I., 2012. On the surface circulation of the Levantine sub-basin derived from Lagrangian drifters and satellite altimetry data. Deep Sea Res. Part Oceanogr. Res. Pap. 65, 46–58. https://doi.org/10.1016/j.dsr.2012.02.008

Millot, C., 1999. Circulation in the western Mediterranean Sea. J. Mar. Syst. 20, 423–442. https://doi.org/10.1016/S0924-7963(98)00078-5

Millot, C., 1985. Some features of the Algerian Current. J. Geophys. Res. 90, 7169-7176. https://doi.org/10.1029/JC090iC04p07169

Millot, C., Taupier-Letage, I., 2005. Circulation in the Mediterranean Sea, in: Saliot, A. (Ed.), The Mediterranean Sea. Springer Berlin Heidelberg, Berlin, Heidelberg, pp. 29–66. https://doi.org/10.1007/b107143

Mkhinini, N., Coimbra, A.L.S., Stegner, A., Arsouze, T., Taupier-Letage, I., Béranger, K., 2014. Long-lived mesoscale eddies in the eastern Mediterranean Sea: Analysis of 20 years of AVISO geostrophic velocities. J. Geophys. Res. Oceans 119, 8603–8626. https://doi.org/10.1002/2014JC010176

Morrow, R., Birol, F., Griffin, D., Sudre, J., 2004. Divergent pathways of cyclonic and anti-cyclonic ocean eddies. Geophys. Res. Lett. 31, L24311. https://doi.org/10.1029/2004GL020974

Morrow, R., Blurmstein, D., Dibarboure, G., 2018. Fine-scale Altimetry and the Future SWOT Mission, in: Chassignet, E.P., Pascual, A., Tintoré, J., Verron, J. (Eds.), New Frontiers in Operational Oceanography. GODAE OceanView. https://doi.org/10.17125/gov2018.ch08

Morrow, R., Carret, A., Birol, F., Nino, F., Valladeau, G., Boy, F., Bachelier, C., Zakardjian, B., 2017. Observability of fine-scale ocean dynamics in the northwestern Mediterranean Sea. Ocean Sci. 13, 13–29. https://doi.org/10.5194/os-13-13-2017

Morrow, R., Le Traon, P.-Y., 2012. Recent advances in observing mesoscale ocean dynamics with satellite altimetry. Adv. Space Res. 50, 1062–1076. https://doi.org/10.1016/j.asr.2011.09.033

Nencioli, F., d'Ovidio, F., Doglioli, A.M., Petrenko, A.A., 2011. Surface coastal circulation patterns by in-situ detection of Lagrangian coherent structures. Geophys. Res. Lett. 38, L17604. https://doi.org/10.1029/2011GL048815

Nencioli, F., Dong, C., Dickey, T., Washburn, L., McWilliams, J.C., 2010. A Vector Geometry–Based Eddy Detection Algorithm and Its Application to a High-Resolution Numerical Model Product and High-Frequency Radar Surface Velocities in the Southern California Bight. J. Atmospheric Ocean. Technol. 27, 564–579. https://doi.org/10.1175/2009JTECHO725.1

Obaton, D., Millot, C., Chabert D'Hières, G., Taupier-Letage, I., 2000. The Algerian current: comparisons between in situ and laboratory data sets. Deep Sea Res. Part Oceanogr. Res. Pap. 47, 2159–2190. https://doi.org/10.1016/S0967-0637(00)00014-5

Onken, R., Robinson, A.R., Kantha, L., Lozano, C.J., Haley, P.J., Carniel, S., 2005. A rapid response nowcast/forecast system using multiply nested ocean models and distributed data systems. J. Mar. Syst. 56, 45–66. https://doi.org/10.1016/j.jmarsys.2004.09.010

Özsoy, E., Hecht, A., Ünlüata, Ü., 1989. Circulation and hydrography of the Levantine Basin. Results of POEM coordinated experiments 1985–1986. Prog. Oceanogr. 22, 125–170. https://doi.org/doi.org/10.1016/0079-6611(89)90004-9

Pascual, A., Bouffard, J., Ruiz, S., Buongiorno Nardelli, B., Vidal-Vijande, E., Escudier, R., Sayol, J.M., Orfila, A., 2013. Recent improvements in mesoscale characterization of the western Mediterranean Sea: synergy between satellite altimetry and other observational approaches. Sci. Mar. 77, 19–36. https://doi.org/10.3989/scimar.03740.15A

Pascual, A., Lana, A., Troupin, C., Ruiz, S., Faugère, Y., Escudier, R., Tintoré, J., 2015. Assessing SARAL/AltiKa Data in the Coastal Zone: Comparisons with HF Radar Observations. Mar. Geod. 38, 260–276. https://doi.org/10.1080/01490419.2015.1019656

Pegliasco, C., Chaigneau, A., Morrow, R., 2015. Main eddy vertical structures observed in the four major Eastern Boundary Upwelling Systems. J. Geophys. Res. Oceans 120, 6008–6033. https://doi.org/10.1002/2015JC010950

Pessini, F., Olita, A., Cotroneo, Y., Perilli, A., 2018. Mesoscale eddies in the Algerian Basin: do they differ as a function of their formation site? Ocean Sci. 14, 669–688. https://doi.org/10.5194/os-14-669-2018

Poulain, P.-M., Menna, M., Mauri, E., 2012. Surface Geostrophic Circulation of the Mediterranean Sea Derived from Drifter and Satellite Altimeter Data. J. Phys. Oceanogr. 42, 973–990. https://doi.org/10.1175/JPO-D-11-0159.1

Puillat, I., Taupier-Letage, I., Millot, C., 2002. Algerian Eddies lifetime can near 3 years. J. Mar. Syst. 31, 245–259. https://doi.org/10.1016/S0924-7963(01)00056-2

Pujol, M.-I., Dibarboure, G., Le Traon, P.-Y., Klein, P., 2012. Using High-Resolution Altimetry to Observe Mesoscale Signals. J. Atmospheric Ocean. Technol. 29, 1409–1416. https://doi.org/10.1175/JTECH-D-12-00032.1

Pujol, M.-I., Faugère, Y., Taburet, G., Dupuy, S., Pelloquin, C., Ablain, M., Picot, N., 2016. DUACS DT2014 : the new multi-mission altimeter dataset reprocessed over 20 years. Ocean Sci. Discuss. 1–48. https://doi.org/10.5194/os-2015-110

Pujol, M.-I., Larnicol, G., 2005. Mediterranean sea eddy kinetic energy variability from 11 years of altimetric data. J. Mar. Syst. 58, 121–142. https://doi.org/10.1016/j.jmarsys.2005.07.005

Rio, M.-H., Pascual, A., Poulain, P.-M., Menna, M., Barceló, B., Tintoré, J., 2014. Computation of a new mean dynamic topography for the Mediterranean Sea from model outputs, altimeter measurements and oceanographic in situ data. Ocean Sci 10, 731–744. https://doi.org/10.5194/os-10-731-2014

Rio, M.-H., Poulain, P.-M., Pascual, A., Mauri, E., Larnicol, G., Santoleri, R., 2007. A Mean Dynamic Topography of the Mediterranean Sea computed from altimetric data, in-situ measurements and a general circulation model. J. Mar. Syst. 65, 484–508. https://doi.org/10.1016/j.jmarsys.2005.02.006

Robinson, A.R., Golnaraghi, M., Leslie, W.G., Artegiani, A., Hecht, A., Lazzoni, E., Michelato, A., Sansone, E., Theocharis, A., Ünlüata, Ü., 1991. The eastern Mediterranean general circulation: features, structure and variability. Dyn. Atmospheres Oceans 15, 215–240. https://doi.org/10.1016/0377-0265(91)90021-7

Robinson, A.R., Hall, P., Leslie, W.G., Baldasserini, G., 2002. Forecasting Synoptic Transients in the Eastern Ligurian Sea. Harvard University, Cambridge.

Robinson, A.R., Leslie, W.G., Theocharis, A., Lascaratos, A., 2001. Mediterranean Sea Circulation, in: Encyclopedia of Ocean Sciences. Elsevier, pp. 1689–1705. https://doi.org/10.1006/rwos.2001.0376

Rogé, M., Morrow, R., Ubelmann, C., Dibarboure, G., 2017. Using a dynamical advection to reconstruct a part of the SSH evolution in the context of SWOT, application to the Mediterranean Sea. Ocean Dyn. 67, 1047–1066. https://doi.org/10.1007/s10236-017-1073-0

Rubio, A., Blanke, B., Speich, S., Grima, N., Roy, C., 2009. Mesoscale eddy activity in the southern Benguela upwelling system from satellite altimetry and model data. Prog. Oceanogr. 83, 288–295. https://doi.org/10.1016/j.pocean.2009.07.029

Sadarjoen, A., Post, F., 2000. Detection, quantification, and tracking of vortices using streamline geometry. Comput. Graf. 24, 333–341. https://doi.org/10.1016/S0097-8493(00)00029-7

Salas, J., Millot, C., Font, J., García-Ladona, E., 2002. Analysis of mesoscale phenomena in the Algerian basin observed with drifting buoys and infrared images. Deep Sea Res. Part Oceanogr. Res. Pap. 49, 245–266. https://doi.org/10.1016/S0967-0637(01)00052-8

Salas, J.D.J., 2003. Evolution of the open-sea eddy ALGERS'98 in the Algerian Basin with Lagrangian trajectories and remote sensing observations. J. Mar. Syst. 43, 105–131. https://doi.org/10.1016/j.jmarsys.2003.08.001

Samelson, R.M., Schlax, M.G., Chelton, D.B., 2014. Randomness, Symmetry, and Scaling of Mesoscale Eddy Life Cycles. J. Phys. Oceanogr. 44, 1012–1029. https://doi.org/10.1175/JPO-D-13-0161.1

Schouten, M.W., de Ruijter, W.P.M., van Leeuwen, P.J., Ridderinkhof, H., 2003. Eddies and variability in the Mozambique Channel. Deep Sea Res. Part II Top. Stud. Oceanogr., Physical Oceanography of the Indian Ocean: from WOCE to CLIVAR 50, 1987–2003. https://doi.org/10.1016/S0967-0645(03)00042-0

Souza, J.M.A.C., de Boyer Montégut, C., Le Traon, P.Y., 2011. Comparison between three implementations of automatic identification algorithms for the quantification and characterization of mesoscale eddies in the South Atlantic Ocean. Ocean Sci. 7, 317–334. https://doi.org/10.5194/os-7-317-2011

[dataset] Stegner, A., Le Vu, B., Pegliasco,C., 2019. Atlas of 3D Eddies in the Mediterranean Sea from 2000 to 2017. https://doi.org/10.14768/2019130201.2

Sutyrin, G., Stegner, A., Taupier-Letage, I., Teinturier, S., 2009. Amplification of a Surface-Intensified Eddy Drift along a Steep Shelf in the Eastern Mediterranean Sea. J. Phys. Oceanogr. 39, 1729–1741. https://doi.org/10.1175/2009JPO4106.1

Taupier-Letage, I., 2008. On the Use of Thermal Images for Circulation Studies: Applications to the Eastern Mediterranean Basin, in: Barale, V., Gade, M. (Eds.), Remote Sensing of the European Seas. Springer Netherlands, pp. 153–164. https://doi.org/10.1007/978-1-4020-6772-3_12

Taupier-Letage, I., 2003. Biological response to mesoscale eddies in the Algerian Basin. J. Geophys. Res. 108. C8, https://doi.org/10.1029/1999JC000117

Testor, P., Send, U., Gascard, J.-C., Millot, C., Taupier-Letage, I., Béranger, K., 2005. The mean circulation of the southwestern Mediterranean Sea: Algerian Gyres. J. Geophys. Res. Oceans 110, C11017. https://doi.org/10.1029/2004JC002861

Theocharis, A., Georgopoulos, D., Lascaratos, A., Nittis, K., 1993. Water masses and circulation in the central region of the Eastern Mediterranean: Eastern Ionian, South Aegean and Northwest Levantine, 1986–1987. Deep Sea Res. Part II Top. Stud. Oceanogr. 40, 1121–1142. https://doi.org/10.1016/0967-0645(93)90064-T

Vargas-Yáñez, M., Plaza, F., Garcıa-Lafuente, J., Sarhan, T., Vargas, J.M., Vélez-Belchí, P., 2002. About the seasonal variability of the Alboran Sea circulation. J. Mar. Syst. 35, 229–248. https://doi.org/10.1016/S0924-7963(02)00128-8

Viúdez, Á., Tintoré, J., 1995. Time and space variability in the eastern Alboran Sea from March to May 1990. J. Geophys. Res. Oceans 100, 8571–8586. https://doi.org/10.1029/94JC03129

Viúdez, Á., Tintoré, J., Haney, R.L., 1996. Circulation in the Alboran Sea as Determined by Quasi-Synoptic Hydrographic Observations. Part I: Three-Dimensional Structure of the Two Anticyclonic Gyres. J. Phys. Oceanogr. 26, 684–705. https://doi.org/10.1175/1520-0485(1996)026<0684:CITASA>2.0.CO;2

Wang, D.-P., 1987. The strait surface outflow. J. Geophys. Res. 92, 10807-10825. https://doi.org/10.1029/JC092iC10p10807

Yi, J., Du, Y., He, Z., Zhou, C., 2014. Enhancing the accuracy of automatic eddy detection and the capability of recognizing the multi-core structures from maps of sea level anomaly. Ocean Sci. 10, 39–48. https://doi.org/10.5194/os-10-39-2014

Zervakis, V., Papadoniou, G., Tziavos, C., Lascaratos, A., 2003. Seasonal variability and geostrophic circulation in the eastern Mediterranean as revealed through a repeated XBT transect. Ann. Geophys. 21, 33–47. https://doi.org/10.5194/angeo-21-33-2003

Zodiatis, G., Drakopoulos, P., Brenner, S., Groom, S., 2005. Variability of the Cyprus warm core Eddy during the CYCLOPS project. Deep Sea Res. Part II Top. Stud. Oceanogr. 52, 2897–2910. https://doi.org/10.1016/j.dsr2.2005.08.020

Figure Caption:

Figure 1 : Averaged Kinetic Energy (KE) associated with **a]** the mesoscale activity (2000 – 2015) and **b]** the mean circulation derived from the MDT. The pink arrows highlight the more energetic pathways of the mean circulation. 4

Figure 2 : *Mean Dynamic Topography (cm) over the Mediterranean Sea and associated closed contours for the mean anticyclonic (orange) and cyclonic (cyan) circulations. The white contours are every 5 cm and the black contour is for 0 cm. The light purple shading represents the bathymetry between the surface and 500 m depth. The main known features are designated as WAG: Western Alboran Gyre; CE: Capraia Eddy; BE: Bonifacio Eddy; PE: Pelops Eddy; WCE: Western Cretan Eddy; IE: Ierapetra Eddy; MM: Mersa-Matruh; RG: Rhodes Gyre; SE: Shikmona Eddy.* 8

Figure 3 : *Mean temporal evolution (solid lines) and associated student errors (shadings) of Radius (top), Amplitude (middle) and EKE (bottom) for main trajectories as a function of normalized lifetime. AEs are red in the ADT and orange in the SLA; CEs are blue in the ADT and cyan in SLA.* 17

Figure 4 : *Percentage of time spent by each pixel of 0.25°x0.25° outside eddies for* **a]** *the ADT and* **d]** *the SLA, within an Anticyclonic Eddy for the* **b]** *ADT and* **e]** *the SLA, and within a Cyclonic Eddy for* **c]** *the ADT and* **f]** *the SLA . Dark tones depict a high occurrence of eddies, white tones highlight areas free of eddies. The MDT closed circulations contours are highlighted in orange for anticyclonic and in light blue for cyclonic.* 20

Figure 5 : *Number of trajectories lasting less than 6 months generated in 1°x1° boxes for* ***a]*** *ADT and* ***b]*** *SLA.* 22

Figure 6 : *Lifetime of the main and merged trajectories lasting longer than 6 months, plotted at the first position of the centers, for* ***a,b]*** *AEs and CEs in the ADT, and* ***c,d]*** *AEs and CEs in the SLA. More than one trajectory can be generated at the same location. The size of the points is also a lifetime indicator (larger disks for longer trajectories).* 23

Figure 7 : *Propagation speed (shading, km/day) and mean direction (arrows) for the AEs detected in* ***a]*** *the ADT and* ***b]*** *the SLA. No information are given if fewer than 25 eddies were detected in a 0.5 x 0.5 grid cell.*..... 24

Figure 8 : *Number of eddies in 0.25°x0.25° boxes (in gray shades) having an opposite rotating sense in the two SSH fields:* ***a]*** *AEs in the ADT corresponding to CEs in the SLA,* ***c]*** *AEs in the SLA corresponding to CEs in the ADT; and having the same rotating sense:* ***b]*** *AEs in both the ADT and the SLA,* ***d]*** *CEs in both the ADT and the SLA. The MDT closed circulations contours are highlighted in orange for anticyclonic and in light blue for cyclonic.* 28

Figure 9 *: Composite ADT* (**a,c**) *or SLA* (**b,d**) *field (in cm) when* **a,b]** *only AEs centers are detected in the ADT field within the box* [26 – 27°E; 33.75 – 34.65°N]*; c***,d]** *no eddy centers are detected within the box in the ADT field. The contours are the MDT every 5 cm (see Figure 2 for the values).*..... 30

Figure 10 *: Monthly percentage of occurrence of SLA features occuring within an ADT AE in the Ierapetra Eddy zone. Orange is reinforcement (AE in SLA), cyan is weakening (CE in SLA), purple is slight displacement (CE and AE in SLA) and green is no change (no eddy in SLA).*..... 31

Figure 11 *: Snapshot of the eddies detected on the 15 Janvier 2003 in a] the ADT and b] the SLA. The yellow contours and points are for AEs, cyan are for CEs. M1, M2 and M3 are three meanders identified in ADT field and reproduced in the SLA field.* 35